Time-resolved study of electron-hole plasmas near the liquid-gas critical point in Si: Evidence for a second condensed phase

L. M. Smith* and J. P. Wolfe
Department of Physics and Materials Research Laboratory, University of Illinois at Urbana-Champaign, Urbana, Illinois 61801
(Received 6 September 1994)

At low temperatures and sufficient densities, free excitons in Si and Ge undergo simultaneous gas-liquid and insulator-metal transitions into droplets of electron-hole liquid. Some previous theoretical and experimental studies have suggested that, under certain values of density and temperature, there may be separate metal-insulator and liquid-gas transitions. In the present paper, we examine the difficult transcritical region for electron-hole liquid formation in unstressed Si using time- and space-resolved photoluminescence spectroscopy. Using the latest models for the luminescence of electron-hole plasma and small excitonic complexes (EC's), we have succeeded in characterizing the complicated luminescence spectra both above and below the liquid-gas critical temperature [$T_c(\mathrm{LG}) \approx 24.5$ K] with a relatively small number of free parameters. Near the liquid-gas critical point the luminescence spectra are analyzed as contributions from four lines: the high-density electron-hole liquid (EHL), a lower-density electron-hole plasma (EHP), free excitons (FE's), and excitonic complexes. After a sufficient thermalization time, the temperature of all phases settles to a value indistinguishable from the lattice temperature. The line shapes of FE's and EC's are calculated using previously established parameters. Using the latest band-renormalization theory, the pair density of the plasma phases (EHL and EHP) determines both the position and the shape of the spectrum. Therefore the analysis of these complex spectra is reduced to five free parameters: A single parameter describing the intensity of the FE line (the intensity of the EC line shape is linked to that of the FE using an experimentally determined scaling relation), the intensities of the two plasma components EHL and EHP, and the pair densities of these two plasmas. These parameters are sufficient to characterize the spectra over a wide range of particle density and temperature. The EHP density obtained in this way is remarkably independent of temperature and particle density, providing evidence for a second condensed phase of electron-hole plasma. The condensed liquid has a density of about one-tenth that of the ground-state electron-hole liquid and is observed both above and below the EHL critical temperature. An excitonic phase diagram for silicon is described which includes two condensed plasmas. A triple point at 18.5 K is observed where the electron-hole liquid coexists with the lower-density condensed plasma (CP) and excitonic gas. Above this temperature the CP is observed at all temperatures up to a second critical point at 45±5 K. We also consider the hypothesis that the extra luminescence attributed to the CP is instead due to large excitonic complexes. Using the recently determined binding energies of large excitonic complexes and the measured gas volume, we conclude that the density of these species is too small to account for the observed luminescence.

I. INTRODUCTION

At low densities, excitons in Si form a nearly ideal gas of noninteracting particles. As the gas density is raised, many-body interactions become important. The details of these interactions determine the form of the excitonic phase diagram. At the highest densities, the many-body problem is well characterized as demonstrated by the success of the theory of the electron-hole liquid (EHL). The intermediate-density regime, however, is not well understood. This is the interesting region where the transition from an insulating excitonic gas to a metallic plasma occurs. At low temperatures this metal-insulator (or "Mott") transition[1] occurs simultaneously with a liquid-gas transition, creating a mixed phase region of metallic droplets and insulating gas of excitons. As the temperature is raised toward the critical point, the saturated gas density of excitons increases by orders of magnitude and the excitons are expected to ionize into a low-density (relative to the EHL) metallic plasma of electrons and holes. The issue of whether this transition is continuous (second order) or discontinuous (first order) has not been previously established.

The ionization of the excitonic gas occurs via screening of the Coulomb interaction between an electron and a hole in the presence of many free carriers. Rodgers, Graboske, and Harwood[2] have determined theoretically that the hydrogenic binding energy vanishes when the screening length is $0.84a_x$, where a_x is the Bohr radius. If one assumes that the Debye-Huckel screening approximation is appropriate [the Debye-Huckel screening length given by $q_{\mathrm{DH}}^{-1}=(8\pi e^2 n/\kappa k_B T)^{-1/2}$, where κ is the static dielectric constant of the material and n is the pair density], one obtains as an estimate of the Mott density

$$n_{\mathrm{DH}}=\frac{(1.19)^2\kappa k_B T}{8\pi e^2 a_x^2} . \quad (1)$$

Estimates such as Eq. (1) indicate that the metal-insulator transition in semiconductors should occur at much lower density than the liquid-gas critical point. This situation is depicted in the standard excitonic phase diagram of Fig. 1, where the dotted line is the Mott density given by Eq. (1) and the solid line is the liquid-gas phase boundary as determined by the universal expression of Guggenheim.[3] Rice,[4] in 1974, suggested that if in such a system the metal-insulator transition were discontinuous, the electron-hole liquid phase diagram would have to be more complex and include the possibility of a second stable plasma phase with density near the metal-insulator transition. Such a phase diagram would have *two* critical points—one for the metal-insulator and one for the liquid-gas transition—and a single triple point, to satisfy the Gibb's phase rule.[5] At the triple point the three phases—liquid, low-density plasma, and excitonic gas—occur simultaneously. Rice adopted this concept of separate first-order metal-insulator and liquid-gas phase transitions from an earlier idea by Landau and Zeldovich[6] for the similar case of expanded metal systems such as mercury. Since 1974 there have been several theoretical attempts[7–11] to calculate the phase diagram for excitons in silicon and germanium, but no study has been able to conclusively determine the true form of the phase diagram for such systems.

Early photoluminescence experiments to determine the phase diagram in silicon were conducted by Shah, Combescot, and Dayem[12] and by Dite, Kulakovskyiĭ, and Timofeev.[13] More recently, studies of the excitonic phase diagram in Si for a variety of stress conditions have been conducted by several groups.[14–16] Typically, intense, short (5–15 ns) laser pulses are used and time-resolved spectra of the recombination luminescence are obtained at temperatures near the liquid-gas critical point. At low temperatures, luminescence from the electron-hole liquid occurs in a broad band of energies well below the relatively sharp free-exciton (FE) line. The EHL luminescence involves a straightforward convolution of the electron and hole Fermi functions and the width of this line is proportional to the sum of electron and hole Fermi energies.[17] The previous workers were able to obtain the EHL density as a function of temperature by such a line-shape analysis and therefore determine the high-density side of the excitonic phase diagram. On the other hand, the exciton line shape depends only on temperature and changes very little with density, and so there is no spectroscopic means to verify the low-density side of the phase diagram.

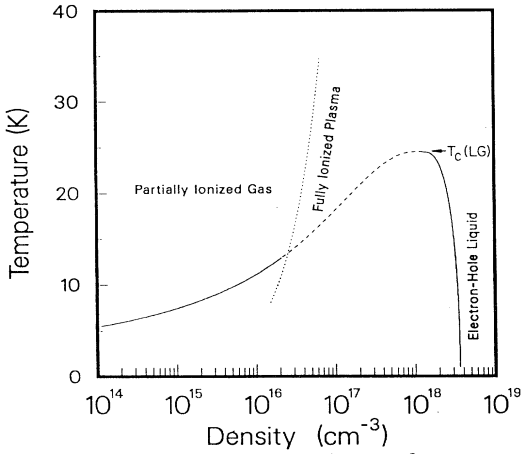

FIG. 1. Standard excitonic phase diagram for unstressed silicon. The solid and dashed line is the Guggenheim (Ref. 3) plot of liquid-gas coexistence densities. The dotted line is the estimate of the Mott density using Eq. (1).

Well below the liquid-gas critical temperature T_c(LG), the gas density is low and the gas is assumed to be composed primarily of excitons. In such a region, the left-hand side of the phase diagram is estimated by the thermodynamic expression of the saturated gas density $n_{\rm sat}(T)=AT^{3/2}e^{-\phi/k_BT}$ (where A is a constant), which depends only on the EHL binding energy, ϕ, measured spectroscopically. This estimate, however, is not valid near T_c(LG), where the gas density is much higher. In this region (dashed line, Fig. 1) the saturated gas changes from a partially ionized excitonic gas to a fully ionized plasma and such simple thermodynamic estimates no longer apply.

Near the liquid-gas critical temperature, the saturated gas is expected to form a pure electron-hole plasma (EHP) and so in principle the gas density can be determined from the position and width of its luminescence spectrum. The difficulty of this approach lies in the complexity of the luminescence spectrum in the critical region. Actual experiments involve inhomogeneous distributions of particle densities. Overlapping contributions from EHL's, EHP's, FE's, and excitonic complexes (EC's) make the determination of the EHP side of the phase diagram a difficult task. Nevertheless, in this work, we attempt to determine both the EHL and EHP phase boundaries by line-shape analysis of the photoluminescence, aided by measurements of the spatial distributions of the specific luminescence components. Our approach is to isolate the spectral shape of each excitonic component by time resolving the luminescence over wide limits. Fortunately, since the previous phase diagram studies, significant progress has been made in understanding the spectral line shapes of various excitonic species. The luminescence from biexcitons in Si is now well characterized[18–20] and it is likely that trions (one electron and two holes or vice versa) will exhibit a similar line shape.[21–25] Also a universal theory for the band-gap renormalization of EHP's has been presented and tested for the case of EHL's.[26] These factors greatly reduce the number of free parameters necessary to describe the composite luminescence spectrum. In addition, we have made spatial measurements of the luminescence in order to obtain the effective volume associated with the excitonic gas. Using this information we present a simplified scheme for isolating contributions of FE's and small (EC's) from the luminescence spectra. We find that when contributions from FE's and EC's are subtracted from the total spectrum, the remaining luminescence can be described by EHL and EHP components.

This spectral and spatial analysis of the recombination luminescence spectrum has uncovered two unusual results.[27–29] First, it is found that EHP density does not follow the expected gas boundary of the phase diagram as

represented by the dashed segment of Fig. 1. Indeed, an EHP component appears only above about 18.5 K and assumes an almost constant density as the temperature is raised. Second, the density of this EHP remains constant as the electron-hole pairs decay in time, indicating a spatial condensation into constant-density droplets. This effect is observed from 18.5 K to above 40 K, which is well above the liquid-gas critical point. The conclusion of this analysis is that a second phase of condensed plasma, distinct from the EHL, exists at higher temperatures. One may interpret this phenomenon as evidence for a separate first-order transition associated with the metal-insulator transition, as predicted by Rice and others. This result is similar to conclusions reached by Schowalter *et al.*[31] for stressed Ge and Simon, Kirche, and Wolfe[32] for unstressed Ge.

At the outset, we point out the possibility that the extra luminescence which we associate with CP may actually arise from other sources. Certainly, a dense EHP is present at early times before the system has completely thermalized. This component evolves smoothly in time and is described well with only a single density as a fit parameter, which fixes both the position and shape of the theoretical line. It is conceivable, however, that at the latest times a combination of luminescence from large excitonic complexes could mimic the EHP luminescence. This interpretation of our data[27,28] has been suggested by Hernandez[30] and by Steele, McMullan, and Thewalt.[33] The latter group used four-particle recombination luminescence to measure the binding energies of larger excitonic complexes (three and four pairs). Using these values and our measurements of the gas volumes in our experiments, we present a simple estimate of the density of large excitonic complexes. The result, given in Appendix C, implies that the number of large complexes is not nearly sufficient to explain the luminescence component we attribute to EHP's. In fact, it is possible that the four-particle recombination spectra reported by Steele, McMullan, and Thewalt[33] also contains an EHP component.

The results of this paper provide a comprehensive description of the recombination luminescence in the transcritical region of Si. The spectra are well characterized with a minimum number of parameters over a wide range of observation times. The simplest assumption of a single density condensed-plasma phase does a remarkably good job of fitting all the many spectra. However, the existence of the CP implies a radical departure from the previously accepted excitonic phase diagram.

In Sec. II we describe our experimental methods. Section III contains our analysis of photoluminescence from the gas phase containing FE's and EC's. This allows us, in Secs. IV and V, to determine the temperature dependence of the plasma phases on the excitonic phase diagram. In Sec. VI we use thermodynamics to calculate the density of the gas phases on the phase diagram. We conclude in Sec. VII with a discussion of the dynamics of the formation and decay of the EHL and the CP.

II. EXPERIMENTAL METHODS

At relatively high temperatures and intermediate densities considerable overlap of the plasma and exciton lines complicates the determination of the plasma density. In order to properly resolve contributions to the luminescence we take advantage of the different lifetimes of these two phases. For example, EHP's have lifetimes of approximately 150 ns, while FE's and associated complexes have lifetimes typically in excess of 1 μs. If time-resolved luminescence is collected over several exciton lifetimes, one can trace the decay of the plasma into the exciton gas and then follow the exciton line shape from near the ionization threshold out to the dilute gas limit.

A cavity-dumped argon ion laser with a 15-ns pulse width and peak absorbed power of approximately 20 W is pulsed every 12 μs and focused to a 30-μm spot onto a polished surface of an ultrahigh purity ($n_A - n_D < 10^{12}$ cm^{-3}) silicon parallelpiped ($3\times4\times1$ mm^3). The sample was mounted inside a variable temperature cryostat with the temperature monitored by a calibrated carbon resistor embedded into the copper base supporting the sample. The temperature measured in this way agreed well with that obtained from the FE line shape. A magnified image of the crystal was focused onto the entrance slit of a spectrometer after being reflected off of two scanning mirrors. The mirrors were attached to galvanometers with orthogonal axes, allowing us to select exactly where luminescence was collected from the crystal. Energy dispersion of the luminescence was accomplished by a Spex $\frac{1}{2}$-m spectrometer with a grating blazed at 1.2 μm and typical resolution of 4 Å. The photons were detected by a Varian VPM-164 phototube operated in photon counting mode. Pulses from the phototube were discriminated and fed to a time-to-pulse height converter which was triggered by the photodetected laser pulse. The arrival time of the photon pulses after the laser pulse were histogrammed using a 512-bin multichannel analyzer (MCA).

A microcomputer controlled the wavelength of the spectrometer, the position of the x and y galvanometers, and the timing data collected by the MCA. Data were taken primarily in two modes. A complete series of time-resolved spectra were obtained after storing a complete 512-point time decay for successive wavelength intervals. Time-resolved spatial scans were obtained by collecting 512-point time decays for successive galvanometer positions. Thus spatial distributions of each phase were determined by selecting a wavelength characteristic of a particular phase. Time-resolved spectral profiles of photoluminescence integrated over the entire volume of the crystal were obtained by collecting photons scattered from the edges of the crystal. In this way the complete spatial or spectral evolution of the photoexcited carriers is determined in a single experiment with 3-ns time resolution and 25-μm spatial resolution. Figure 2 shows examples of time-resolved spectral and spatial experiments at 14.5 K using the methods described above.

III. EXCITON GAS NEAR IONIZATION

As noted before, the high-temperature plasma lines overlap strongly with the exciton lines, and so in order to obtain the plasma density from line shape analysis it is necessary to completely understand the exciton line shape

as the carrier density is increased to near the ionization threshold. The theoretical line shapes of the excitonic phases have been calculated as follows.

(i) The theoretical energy distribution of the (FE's) is $\sqrt{E}\exp(-E/k_BT)$, as derived from a Maxwell-Boltzmann distribution of particles.[34] Here E represents the kinetic energy of the radiatively decaying particle and T is the measured lattice temperature. Overlap of the LO-TO phonon replicas has been included assuming a splitting of 1.8 meV. The ratio of the LO to TO replica amplitudes has been fixed at 11%, as determined by Hammond, Smith, and McGill.[35] The validity of this simple line-shape analysis is shown in Fig. 3(c).

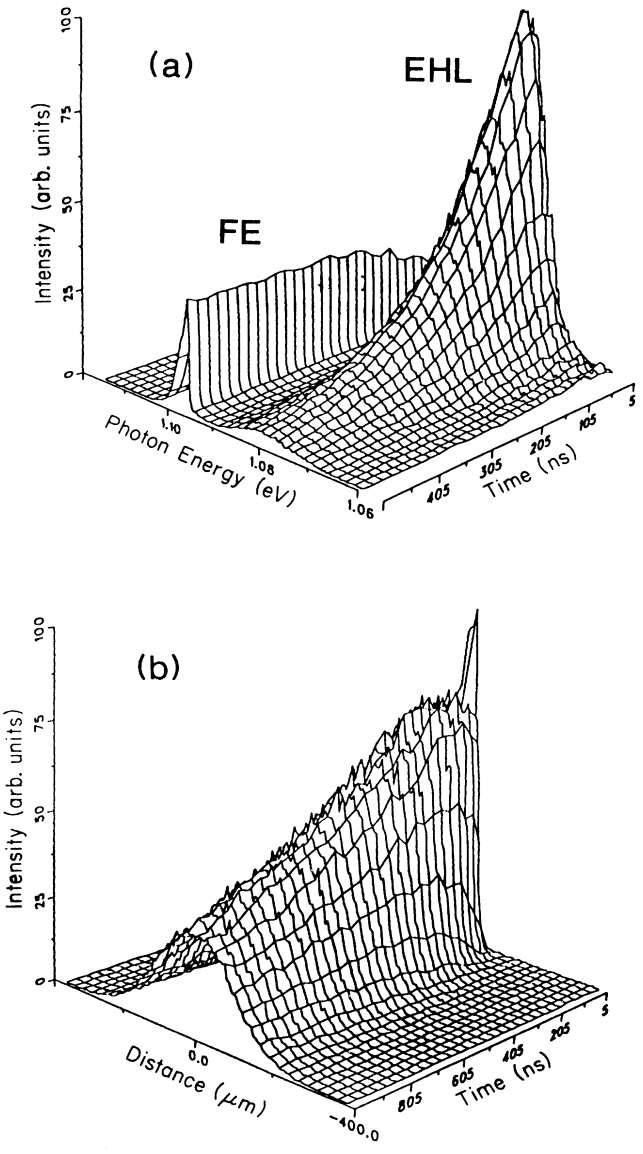

FIG. 2. Pseudo-three-dimensional graphs of time-resolved photoluminescence collected in two modes. (a) 14.5 K spectra showing decay of the EHL luminescence (broad feature centered at about 1.08 eV) and the rise of the free-exciton line (sharp line centered at 1.10 eV). (b) 14.5 K spatial scan showing an expansion of the FE with time. The spatial distribution at $t=0$ ns is about 30 μm wide and expands to over 200 μm within the first microsecond.

(ii) We have included the possibility of three- and four-particle complexes in our analysis. The molecule and trion line shapes are calculated following Cho's theory.[18] The molecular line shape has been well determined in both stressed[19] and unstressed[20] Si experiments. Performing a theoretical fit to Thewalt's spectra of excitonic molecules (EM's) in unstressed Si at 2 K,[20] we determine an EM binding energy of 1.22 meV and a broadening parameter of 1.0 meV. Theoretical estimates of the trion binding energy[21–23] indicate that the three-particle complex (two electrons and one hole, or vice versa) has a binding energy in the range of the excitonic molecule binding energy. In addition, Cho's line shape[18] is not very sensitive to the mass of the recoiling particle[24,25] and so luminescence from the trion and biexciton are likely to be very similar. Thus we use the known biexciton line shape to also represent trions and identify this luminescence component as small (EC's). As in the case of the free exciton we include LO and TO phonon replicas using the same energy splitting and amplitude ratio as before.

At sufficiently long times after the laser pulse, the plasma phases have decayed, leaving only the gas phases, FE's and EC's. Representative luminescence spectra at 28 K are plotted in Fig. 3. Note that at 2000 ns after the laser pulse, the luminescence can be exactly fit by a simple Maxwell-Boltzmann exciton line shape at the lattice temperature. At somewhat earlier times (600 and 1200 ns in Fig. 3) when the gas density is higher, a tail appears on the low-energy side of the exciton luminescence. We now discuss several possible explanations for this result.

First we consider the possibility that the low-energy tail is the result of exciton-exciton or exciton-free carrier collisions.[36] Collision broadening should widen the exciton line on both the low- and high-energy sides. If enough broadening is included to fit the low-energy distortion, however, the broadened exciton line is too wide on the high-energy side to fit the upper portion of the exciton luminescence. Similarly, if a combination of exciton and plasma line shapes are summed to account for the low-energy broadening, it again becomes impossible to fit the high-energy portion of the luminescence.

Finally, we consider the possibility that the low-energy tail is from small excitonic complexes. We find that the previously determined biexciton line shape fits the low-energy tail perfectly, with only intensity as an adjustable parameter. In Figs. 3(a) and 3(b) the thin lines are the FE and EC components and the open circles are the summation of these two line shapes. These two components, FE's and EC's, describe the luminescence over a remarkably wide range of carrier density.

An identification of the type of complex contributing to the EC luminescence line can be gained from thermodynamics. One can estimate the relative exciton and complex densities by dividing the luminescence intensity of each line by the effective volume from which the luminescence originates inside the crystal. This is easily accomplished by determining the exciton and complex line intensities from the spectra at the photon energies

noted by the arrows in Fig. 3 and collecting time-resolved spatial scans at those same spectral positions. The spatial expansion of excitons at 28 K is shown in Fig. 4.

If a diffusive process determines the expansion of the excitons and complexes, then a plot of the square of the diameter of the spatial distribution with time should be linear. In Fig. 5 the square of the spatial full width at half maximum for FE's and EC's is plotted as a function of time. In both cases the spatial expansion is indeed diffusive. A diffusion constant $D=43$ cm^2/s is obtained for the excitons at 28 K, which is consistent with previously determined values obtained by others.[37–40] The instantaneous ratio of Δ^2 for the two species is about 2. For local equilibrium, this is the ratio expected for excitons and biexcitons.

The relative densities of the FE's and EC's can now be calculated by dividing the intensity of each line by the volume each species occupies in the crystal. The variation of the EC density with the FE density is plotted in Fig. 6. The EC density varies almost exactly with the $\frac{3}{2}$ power of the FE density, suggesting that the luminescence from the low-energy edge of the exciton line is due mostly to three-particle complexes, the trions. However, biexcitons should exhibit only a slightly steeper density dependence, namely, $n_{EM} \propto n_{FE}^2$. Considering also the Δ^2 ratio, we suspect that both biexcitons and trions are contributing to the EC luminescence line. Previously, the existence of trions has been reported by Thomas and coworkers for unstressed germanium.[24,25]

Regardless of the precise composition of the exciton gas, the empirical scaling relation observed in Fig. 6 is a very useful result. The measured relation between the FE and EC densities allows us to predict rather accurately the relative intensities of the corresponding spectral components. For given excitation conditions, the EC and FE luminescence spectra are characterized by a single adjustable parameter, the intensity of the FE component. This procedure will be used to separate overlapping gas and plasma components.

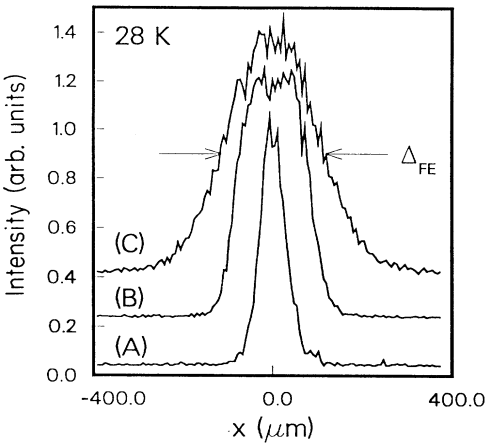

FIG. 4. Time-resolved spatial distributions at 28 K of the free excitons at 10, 100, and 1000 ns. Arrows mark the full width at half maximum of the 1000-ns distribution.

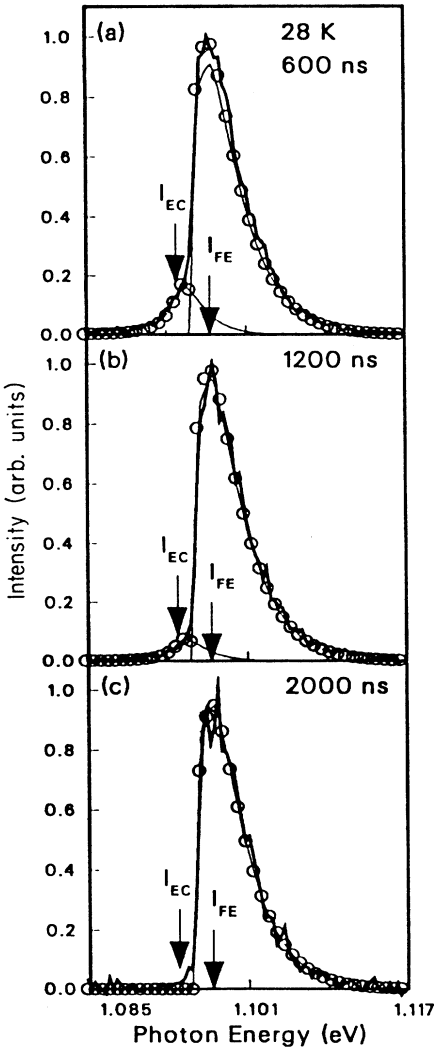

FIG. 3. Time-resolved luminescence spectra at $T=28$ K. Open circles are the sum of FE and EC components (fine lines). (a) 600 ns after laser pulse. (b) 1200 ns after laser pulse. (c) 2000 ns after laser pulse.

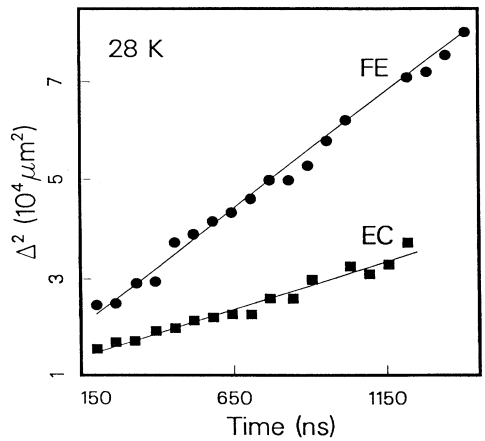

FIG. 5. Plot of Δ^2 vs time at 28 K for free excitons (FE, circles) and excitonic complexes (EC, squares), demonstrating a diffusive expansion of these species.

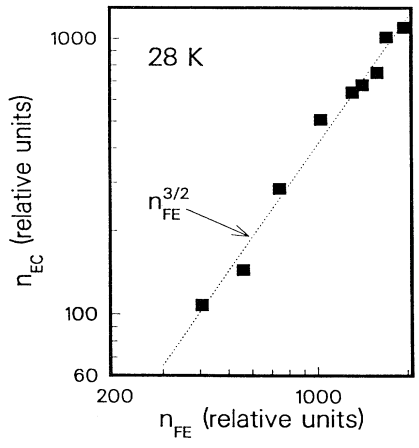

FIG. 6. Plot of relative changes of the excitonic complex and free excitonic densities at 28 K. The dotted line is $n_{EC} \propto n_{FE}^{3/2}$.

IV. THE PLASMA PHASES BELOW THE LIQUID-GAS CRITICAL TEMPERATURE

Special care must be taken in calculating electron-hole plasma line shapes. Fortunately, the spectral contribution from one form of EHP, namely, the EHL, is completely isolated from those of other excitonic species at low temperatures. An EHL spectrum at 14.5 K is shown in Fig. 7(a). A simple convolution[17] (dashed line) of the electron and hole densities of states gives a reasonable approximation to the data, but does not account for the low-energy tail of the luminescence from the EHL. A significant improvement (open circles) in the fit to the experimental data is achieved by broadening the electron and hole density of states. Here we utilize a phenomenological model which is similar to the theory of Landsberg,[41–44] but with a temperature- and density-independent broadening (see Appendix A). The LO and TO phonon replicas are included in the analysis with the intensity ratio of 11%.[35] Both the spectral position (shown below) and the broadening (Appendix A) are calibrated by a theoretical fit to the 14.5 K EHL spectrum of Fig. 7(a). The purpose of these procedures is to enable us to accurately generate the spectral line shape of the EHP in unstressed Si given only the plasma density and temperature.

In general, the spectral position of EHP luminescence shifts to lower energy with increasing density. This redshift results from reduction of the band gap due to Coulomb interactions between the charged carriers. The shift of the band gap with density is related to the sum of the exchange and correlation contributions to the free energy of the plasma by the simple derivative

$$\Delta E_{BB} = \frac{\partial(nF_{xc})}{\partial n} \ . \tag{2}$$

Here $\Delta E_{BB} = E_g' - E_g$ is the difference between the unrenormalized (E_g) and renormalized (E_g') band gaps, n is the density of the plasma, and F_{xc} is the sum of the exchange and correlation energies. Vashishta and Kalia[26] (VK) have calculated F_{xc} for degenerate plasmas at $T=0$ K and have determined that this sum obeys the following universal form, which is independent of band structure:

$$F_{xc} = \frac{-4.8316 - 5.0879 r_s}{0.0152 + 3.0426 r_s + r_s^2} \Delta_x^0 \ , \tag{3}$$

where $r_s = (3/4\pi n a_x^3)^{1/3}$, $a_x = \kappa\hbar^2/\mu e^2 = 49$ Å is the theoretical exciton Bohr radius, and $\Delta_x^0 = \mu e^4/2\kappa^2\hbar^2 = 12.85$ meV is the theoretical exciton binding energy. The energy shift of the band gap with density using Eqs. (2) and (3) for EHP's in silicon is shown as the solid line in Fig. 7(b). One can calibrate this result by noting that the low-energy onset of the plasma luminescence is just the renormalized band gap minus the TO phonon energy:

$$E_{BB} = E_g - \Delta E_{BB} - \hbar\omega_{TO} \ , \tag{4}$$

where $\hbar\omega_{TO}$ is the TO phonon energy.

Photoluminescence data of EHL's at 14.5 K are shown in Fig. 7(a), with open circles displaying the best fit to the data with EHL density equal to 3.0×10^{18} cm^{-3}. The band bottom E_{BB} of the EHL luminescence is marked

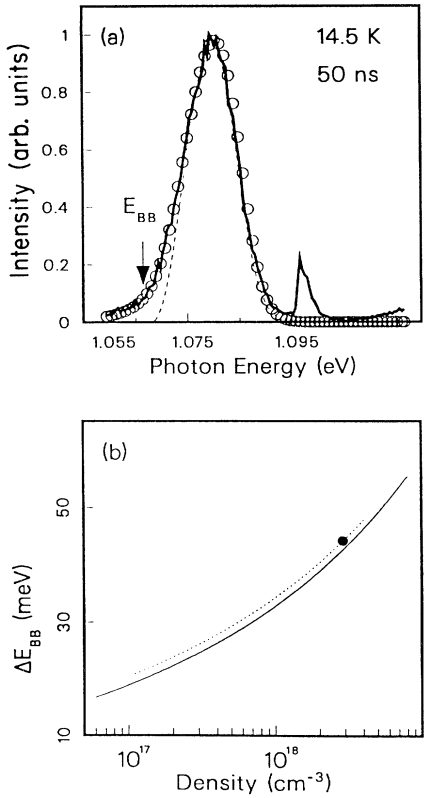

FIG. 7. (a) 14.5 K luminescence spectra used to calibrate the VK calculation. Open circles are the theoretical EHL line shape for a liquid of density 3.0×10^{18} cm^{-3}. The dashed line is the corresponding best fit achieved using an unbroadened line shape (no Landsberg broadening) with a fit density 2.8×10^{18} cm^{-3}. (b) Theoretical calculations of the band-gap renormalization as a function of electron-hole pair density. The solid line is $T=0$ K calculation of Vashishta and Kalia (Ref. 26) [Eqs. (2) and (3) in the text]. The closed circle is the experimentally determined band renormalization for the 14.5 K liquid in (a). The dotted line shows a rigid shift of the Vashishta-Kalia expression [Eqs. (2) and (3)] by 1.53 meV, to agree with the data.

with an arrow. Thus a fit to the EHL luminescence data allows us to determine the renormalized band gap for a particular density. The energy shift determined in this manner is shown as the data point in Fig. 7(b). The expression of VK [Eq. (3)] is found to underestimate the renormalization by about 1.53 meV. Thus, to obtain a more accurate semiempirical expression for $E_{BB}(n)$, we add a constant correction of 1.53 meV to the VK expression. The dashed line in Fig. 7(b) shows this calibrated band-gap shift, which will be used in our analysis to position the theoretical plasma line shapes for each density.

Actually, Vashishta and Kalia[26] calculate the band-gap renormalization at zero temperature in the limit of high degeneracy. In this paper, however, we use their results to analyze luminescence from nonzero temperature plasmas with densities covering the entire range from strong degeneracy to nondegeneracy. In Appendix B we explore the validity of the VK results for the density and temperature ranges of use in these experiments. We estimate that errors in density originating from the VK expression are less than 15% and do not significantly change our results.

In our time-resolved experiments, which employ 10-ns laser pulses, the EHP cools rather quickly (<25 ns) to the lattice temperature, which is controlled in the experiment (see Sec. VII). Thus, after this thermalization period, the EHP luminescence line shape and energy position are completely determined by only one free parameter—the plasma density.

The existence of EHP's with density lower than the EHL is indicated in the spectrum of Fig. 8(a). This spectrum at 21.7 K corresponds to the dashed region on the phase diagram, Fig. 1, where both the EHL and ionized gas (EHP) are expected to appear. Consequently, such spectra are among the most complex which we must analyze. An EHL line with density 2.3×10^{18} cm^{-3} and $T=21.7$ K explains the low-energy side of the luminescence, as indicated by the fine curve at the far left. Also the high-energy side of the spectrum is fit well by a FE line shape with $T=21.7$ K, as shown by the fine curve at the far right. This sharp luminescence peak comes from excitons which have diffused into a lower-density region of the crystal during the 150-ns delay time. Using the scaling law measured for excitonic complexes (Sec. III), we show also the corresponding EC line shape.

Clearly, there is a significant component of "extra luminescence" (shaded region). To isolate this extra luminescence, we subtract the EC and FE gas components, leaving the spectrum of Fig. 8(b). The addition of an EHP spectrum with $n=2.4\times10^{17}$ cm^{-3} and $T=21.7$ K appears to explain this luminescence well. The open circles show the resulting least-squares fit to the data using only four free parameters: the density and the intensity of EHP's and EHL's.

Following this procedure, we analyze plasma luminescence at temperatures near the EHL critical point in order to determine the densities of the plasma phases. In Fig. 9 luminescence data taken at 50 and 150 ns with FE and EC luminescence subtracted are displayed at various temperatures. The densities determined from theoretical fits to these and similar spectra taken at various temperatures are shown as circles on the phase diagram in Fig. 9(i). The solid circles correspond to the spectra displayed.

In the 17.6 K data, well below the liquid-gas critical temperature, only a single high-density electron-hole plasma line shape (EHL) is necessary to describe the luminescence. The EHL density at this temperature is 2.8×10^{18} cm^{-3} for both the 50- and 150-ns spectra [Figs. 9(a) and 9(b)], with only the intensity decreasing with time. This is characteristic of photoluminescence from EHL droplets—only the number of pairs in the droplets (and thus the luminescence intensity) decreases, while the thermodynamically established density remains fixed. The density of the EHL conforms closely with the temperature dependence expected for a simple liquid using the universal expression of Guggenheim shown as the solid line in the phase diagram of Fig. 9(i).

At temperatures above 18.5 K, the data can no longer be explained by a single EHL line shape, but fits can be

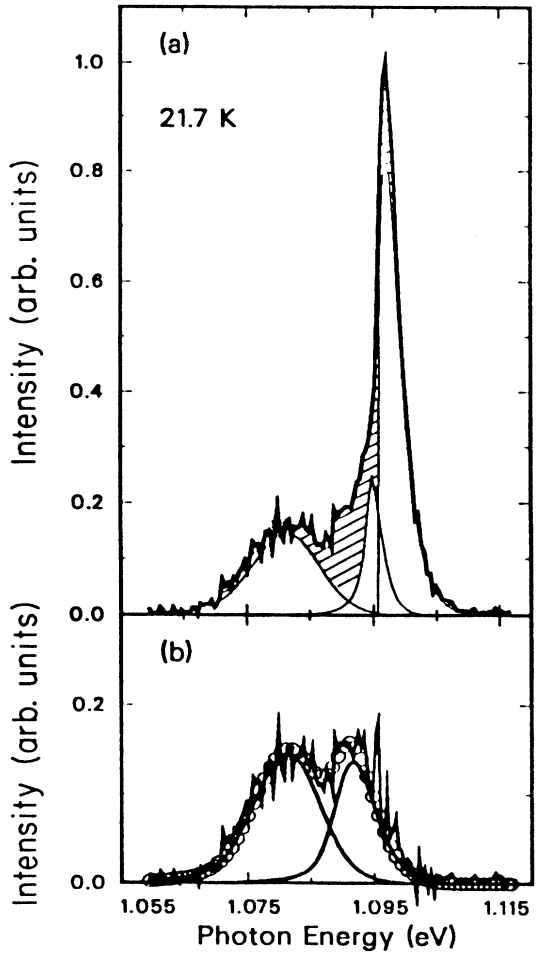

FIG. 8. Time-resolved spectra 150 ns after the laser pulse. (a) 21.7 K spectrum. (b) 21.7 K spectrum with FE's and EC's subtracted as described in the text (bold solid line). Open circles are the sum of EHL and EHP line shapes (light lines) giving the best fit to the data.

achieved with the addition of a second EHP line of lower density. For example, the 19.7 K data of Figs. 9(c) and 9(d) is too wide to be explained by a single plasma line shape. However, the combination of two plasma lines of density 2.5×10^{18} and 2.4×10^{17} cm^{-3} can account for both the 50- and 150-ns spectra. The EHL and EHP luminescence line shapes remain fixed between these two times, while only their relative intensities change. At these temperatures the densities of the EHL and EHP fall near the Guggenheim curve [solid line in Fig. 9(i)]. The estimated accuracy of the densities of these two plasma components determined from the spectral fits is of the order of the size of the solid circles, so no error bars are shown.

As the temperature is raised from 17.6 to 19.7 K, the EHL density decreases along the high-density side of the Guggenheim curve. The plasma density, however, appears to depend very little on temperature and does not

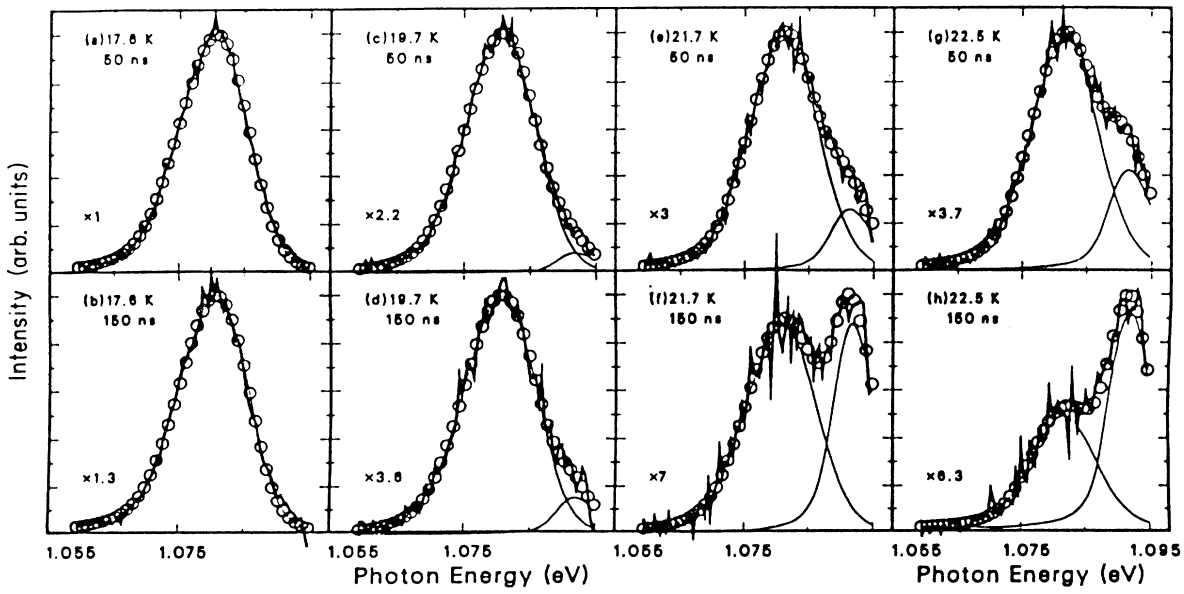

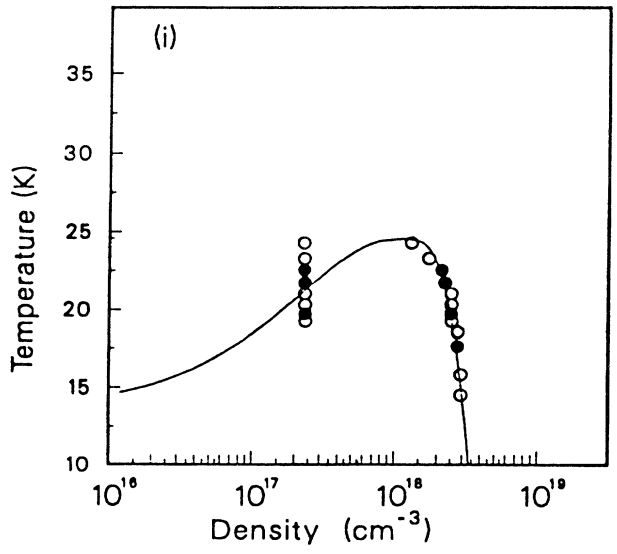

FIG. 9. Time-resolved photoluminescence spectra 50 and 150 ns after the laser pulse with EC and FE components subtracted as in Fig. 8. Open circles are the sum of EHL and/or EHP line shapes (light lines) giving the best fit to the data. The parameters are as follows: (a) 17.6 K, 50 ns; (b) 17.6 K, 150 ns; (c) 19.7 K, 50 ns; (d) 19.7 K, 150 ns; (e) 21.7 K, 50 ns; (f) 21.7 K, 150 ns; and (g) 22.5 K, 50 ns; (h) 22.5 K, 150 ns. (i) Densities of the EHL and the EHP (closed circles) obtained from fits (a)–(h) are displayed on a Guggenheim (Ref. 3) plot of the phase diagram with $T_c=24.5$ K and $n_c=1.15\times10^{18}$ cm^{-3}. Open circles are the results of a line-shape analysis at other temperatures.

increase as expected for simple liquid-gas coexistence. This behavior continues to persist at higher temperatures, as can be seen in the 22.5 K data in Figs. 9(e) and 9(f). This represents a significant departure from the expected behavior of the gas phase in the EHL critical region.

As has been observed previously,[45] the electron-hole liquid forms from a hot plasma, which is created initially by the excitation pulse. The excitation powers used in our experiments are sufficiently low that the liquid condenses from a lower-density plasma. As the hot plasma thermalizes and condenses into a high-density liquid, the band bottom should quickly move to lower energies due to the increased band renormalization. Since this process does not occur at lattice temperatures above the critical point, this effect suggests a method to accurately determine the liquid-gas critical temperature without spectral analysis.

The renormalized band bottom is experimentally estimated as shown in Fig. 10(a). The time dependence of the onset energy is a measure of the temporal change in the plasma density, i.e., $h\nu_{\text{onset}} \sim E_{BB}(n)$. In Fig. 10(b) such data are plotted at 24.2 and 25.2 K. A remarkable change in the time evolution of the band bottom is observed with only one degree change in the lattice temperature. At 24.2 K [squares in Fig. 10(b)] the low-energy edge decreases rapidly with time until a stable high-density liquid is established at ≈ 40 ns. In contrast, the 25.2 K data [circles in Fig. 10(b)] exhibit virtually no change in the low-energy edge of the luminescence during thermalization and gradually increase with time. Thus we estimate the EHL critical temperature to be T_c (LG) $\approx 24.5 \pm 0.5$ K, which is between the results of Forchel *et al.*[14] (23 K) and Shah, Combescot, and Dayem[12] (27 K) and Dite, Kulakovskiĭ, and Timofeev[13] (28 K).

In Fig. 11, complete 150-ns luminescence spectra are shown over the entire EHL critical region. Note the stability of the low-density EHP line (shaded), even while the position of the EHL line shifts to higher energies as the temperature is raised. The EHL density decreases as the critical point is approached and nicely displays the expected temperature dependence for a simple liquid. In contrast, the EHP density is temperature independent and does not increase to the EHL critical density as the temperature is raised toward the liquid-gas critical point. Remarkably, even at 25.2 K, which is above T_c(LG), this same low-density plasma line is observed to contribute to the spectra.

What is the nature of the plasma producing this luminescence? Is the low-density plasma a stable phase even above the EHL critical point? In the next section we look at the time evolution of the luminescence after the initial excitation from the laser pulse and observe the relaxation of this unusual plasma.

V. THE PLASMA PHASE ABOVE THE LIQUID-GAS CRITICAL TEMPERATURE

Photoluminescence spectra observed above the liquid-gas critical point are actually simpler than those below T_c(LG). After subtraction of the FE and EC line shapes,

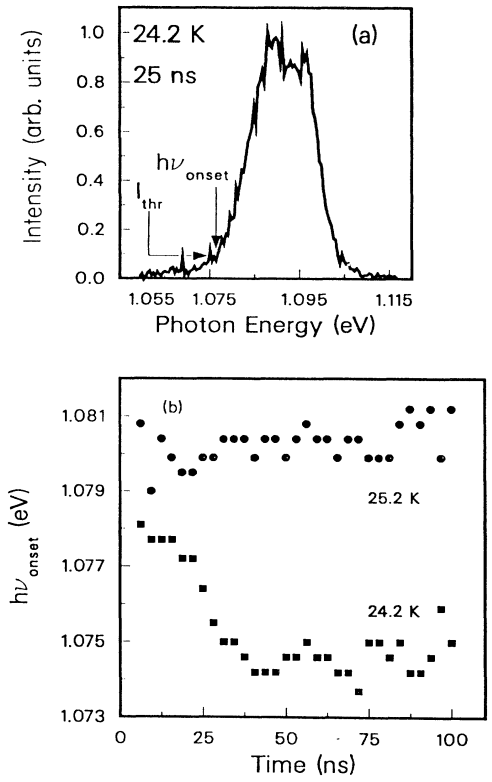

FIG. 10. (a) Time-resolved luminescence spectrum at 24.2 K and 25 ns. $h\nu_{\text{onset}}$ is determined by the photon energy at which the threshold intensity I_{thr} is exceeded. (b) $h\nu_{\text{onset}}$ versus time after the beginning of the laser pulse. The onset energy determined for I_{thr} is equal to 10 times the background. A significant drop in the low-energy edge with time at 24.2 K marks the condensation of the EHL. (The low-energy edge of the luminescence decreases monotonically with increasing density.)

all the luminescence can be described using only a single EHP line shape at each delay time, as shown in Fig. 12. The error bars in Fig. 12(b) denote 20% changes in the minimum χ^2 of the fit. The arrows mark the band bottom energy of the luminescence. The density of the plasma decreases with time as can be seen by the shift of the luminescence to higher energy. For times >25 ns the luminescence is well described by the lattice temperature. By 150 ns the plasma density decreases to $\approx 2.3 \times 10^{17}$ cm^{-3}. The remarkable feature is that for all times after 150 ns the luminescence can be fit by plasma luminescence of the same density [see Fig. 12(b)], while the intensity drops by nearly an order of magnitude. To maintain a constant density plasma while the number of particles decreases, a spatial condensation must be occurring. Since the spatial profiles of the plasma luminescence are actually observed to increase during this period, due to phonon wind forces,[38–40] we conclude that the plasma must form droplets. We refer to this new constant density phase as the condensed plasma (CP).

As noted before, this second plasma phase exists also below the critical temperature for EHL condensation, actually down to 18.5 K. The relaxation time for the CP to come to its equilibrium density is considerably shortened

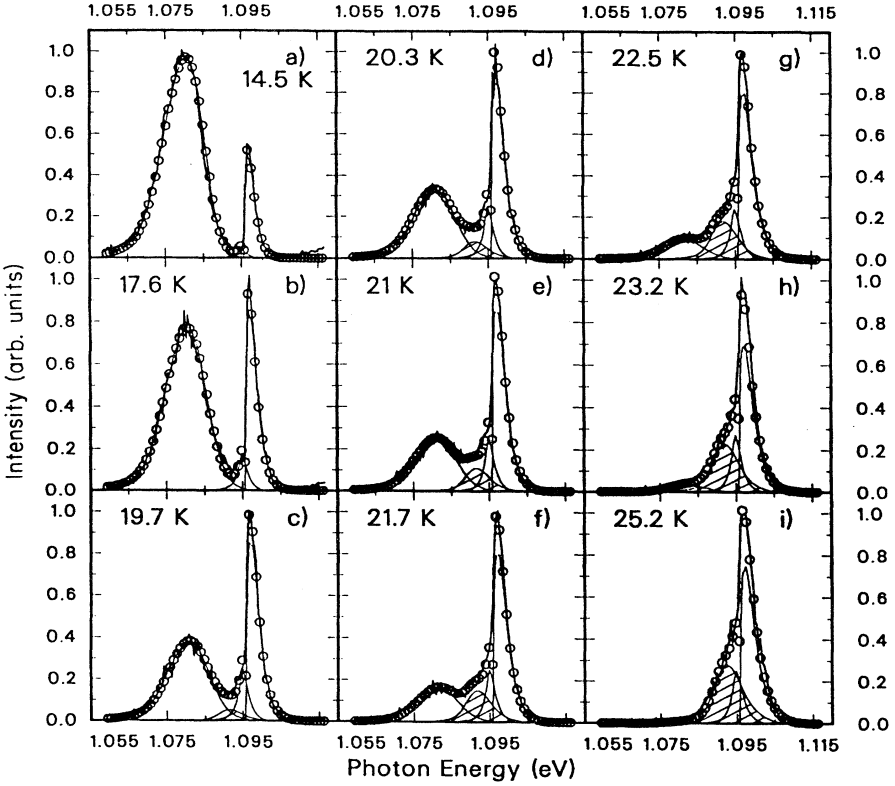

FIG. 11. Luminescence spectra 150 ns after the laser pulse. Open circles are composed of EHL, CP, EC, and FE components, shown in order of increasing energy position. Luminescence from the new condensed phase is shaded. Densities of the EHL and CP phases may be found in Fig. 10(i). The parameters are (a) 14.5 K, (b) 17.6 K, (c) 19.7 K, (d) 20.3 K, (e) 21.0 K, (f) 21.7 K, (g) 22.5 K, (h) 23.2 K, and (i) 25.2 K.

in the presence of an EHL, i.e., less than about 50 ns. This is understandable because the rapid condensation of EHL droplets is an effective means of lowering the surrounding plasma density. Above the liquid-gas critical temperature, an EHL is no longer formed and so the only way the average gas density can be reduced is through spatial expansion and decay of the carriers. This process is much slower and so it takes nearly 150 ns for the equilibrium CP phase to be formed.

The critical point for the formation of the low-density condensed plasma phase is observed by performing similar analysis of plasma luminescence in the temperature range 24.5–45 K. The density obtained from spectral fits of this luminescence is displayed in Fig. 13. The plasma density determined from spectroscopic analysis of luminescence data at 28, 35, and 40 K is observed to decrease within 150 ns to a constant value. Plasma densities at 45 K, however, steadily decreases to lower density until no plasma luminescence is present. This behavior can be seen directly when comparing the 40 and 45 K photoluminescence spectra of Fig. 14. The dashed line is for reference and marks the photon energy 1.095 eV. Note that the positions of the peak intensity and the low-energy edge of the luminescence at 40 K do not change with time after 150 ns. However, the 45 K data exhibit markedly different behavior. The positions of the peak intensity and low-energy edge of the luminescence shift to higher energies over the same time interval. At this temperature, therefore, the plasma appears to decay homogeneously. The plasma density decreases as the volume expands and the carriers decay, indicating that the plasma is no longer condensed.

Electron-hole liquid does not fill the volume from which luminescence is detected, but instead forms a cloud of droplets. The ratio of liquid volume to cloud volume is the filling fraction f. For example, the filling fraction of a homogeneous plasma is unity by definition, while that for EHL droplets at low temperature is typically 1% or less. The relative change in the filling fraction of the CP can be computed by noting that the spatially integrated plasma luminescence intensity I depends on the density and volume as $I \propto fn^2V$, where f is the fraction of the volume V occupied by plasma of density n. Here we assume that nfV is the total number of pairs in the plasma and the radiative decay rate is proportional to n. We compute the relative change in the filling fraction by dividing the intensity I by the square of the fit density n and the volume V the plasma is observed to occupy in the crystal. In Fig. 15 the relative change in the filling fraction at times after 150 ns is shown. For the temperatures 28, 35, and 40 K, the filling fraction decreases by an order of magnitude over the lifetime of the CP. However, at 45 K the filling fraction is observed to remain relatively constant, within the errors of our measurements. This is exactly consistent with our conclusion that the plasma above 45 K is not condensed, but merely decreases in density with time through particle decay and spatial expansion into the crystal.

A summary of EHL and CP luminescence at temperatures between 14.5 and 40 K is shown in Figs. 16(a)–16(g). All spectra are taken 150 ns after the laser pulse to ensure that the plasma above T_c(LG) has relaxed

to the equilibrium CP density. Only a single spectral line shape (EHL) is necessary to explain the photoluminescence at temperatures below 18.5 K. Both EHL and CP luminescence line shapes are seen in spectra at temperatures between 18.5 and 24.5 K. Above 24.5 K the CP line is consistent with all the data up to 40 K. Densities of the EHL and CP phases determined from these and other spectral fits are shown on the phase diagram of Fig. 17 as closed circles. In this figure, the triangles represent EHL data by Hammond and co-workers and the open circles are estimates of the gas density as described in Sec. VI. In the remainder of this section we examine in detail the temperature dependence of several important EHL and CP properties.

It is well known theoretically[46–48] and experimentally[14,15,49] that the following equilibrium parameters of the EHL at low temperatures exhibit a quadratic temperature correction:

$$n_{\mathrm{EHL}}(T)=n_{\mathrm{EHL}}(0)-\alpha T^2 ,$$
$$E_F^{\mathrm{EHL}}(T)=E_F^{\mathrm{EHL}}(0)-\beta T^2 , \quad (5)$$
$$\phi_{\mathrm{EHL}}(T)=\phi_{\mathrm{EHL}}(0)+\delta T^2 ,$$

where n_{EHL}, E_F^{EHL}, and ϕ_{EHL} are the density, Fermi energy, and EHL exciton work function, respectively, and α, β, and δ are independent of temperature. These parameters are directly determined from the spectral fits. We find in Figs. 18(a)–18(c) that the EHL exhibits this predicted behavior (solid lines) for temperatures below 20 K, though significant deviation from theory occurs as T_c(LG) is approached. If we make a series expansion of the free energy and keep terms only up to quadratic in the temperature, we can write

$$F(T)=\varepsilon_0(n)-\tfrac{1}{2}\gamma T^2 , \quad (6)$$

where ε_0 is the EHL ground-state energy at $T=0$ and γ is independent of temperature. The results of Eq. (5) follow directly from this and should be valid as long as the expansion of the free energy is valid, namely, as long as $k_B T \ll E_F$. Therefore, since the CP phase is nondegenerate, one would expect that higher-order corrections are

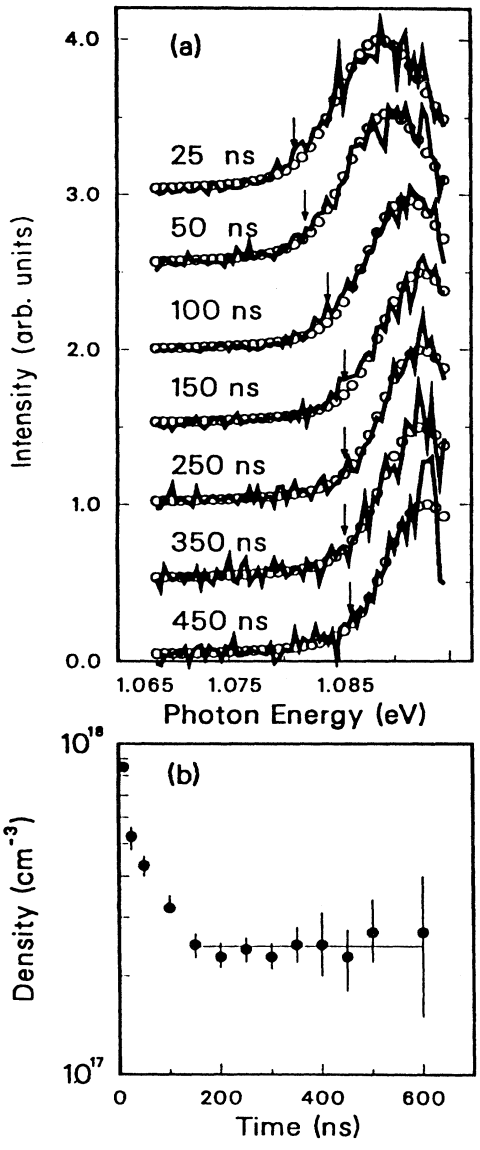

FIG. 12. (a) Time-resolved luminescence spectra at $T=28$ K with FE and EC components subtracted. Open circles are the least-squares fit to the data with arrows marking the "band bottom" energy of each spectra. (b) Plasma density vs time obtained from (a). Error bars denote a 20% variation in the minimum χ^2 of the spectral fit.

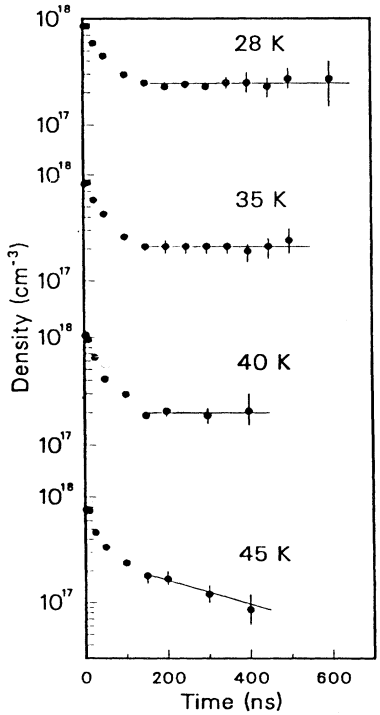

FIG. 13. EHP density vs time at 28, 35, 40, and 45 K obtained by least-squares fits of time-resolved spectra as in Fig. 12.

needed in Eqs. (5) and (6). Remarkably, if one plots n_{CP}, E_F^{CP}, and ϕ_{CP} versus T^2 [see Figs. 17(d)–17(f)], one finds that the same quadratic temperature dependence holds for the equilibrium parameters of the CP phase. We can therefore summarize all of our results for the EHL and CP phases quite succinctly:

$$n_{EHL}(T)=(3.36-1.8\times10^{-3}T^2)\times10^{18}\ \text{cm}^{-3}\ ,$$
$$E_F^{EHL}(T)=22.4-10.7\times10^{-3}T^2\ \text{meV}\ , \quad (7)$$
$$\phi_{EHL}(T)=8.21+5.8\times10^{-3}T^2\ \text{meV}\ ,$$

for $T<20$ K and

$$n_{CP}(T)=(2.48-2.6\times10^{-4}T^2)\times10^{17}\ \text{cm}^{-3}\ ,$$
$$E_F^{CP}(T)=3.52-8.2\times10^{-3}T^2\ \text{meV}\ , \quad (8)$$
$$\phi_{CP}(T)=6.8+7.5\times10^{-3}T^2\ \text{meV}\ ,$$

for $18.5<T<45$ K. The adequacy of the T^2 correction terms in describing the CP equilibrium properties is unexpected, but provides a simple means of parametrizing the data.

In summary, our analyses of the photoluminescence have shown that the phase boundaries of the liquid and plasma cannot be explained by standard liquid-gas coexistence theory. A phase diagram with *two* condensed phases and consequently two critical points at 24.5 and 45 K is indicated. We note that at all temperatures where both the EHL and CP phases can exist, luminescence from each phase is present. This is not what is expected for a homogeneous system, but it must be remembered that the experimental carrier distributions are not in equilibrium over the entire volume occupied by the carriers. In fact, the average carrier density varies locally from a high value close to the excitation center, down to zero far away from the laser spot. Only a local quasiequilibrium can be defined. The range of carrier densities present in the crystal extend over the entire phase diagram and so luminescence from all phases are possible. Thus, from the data we can only infer a triple-point temperature as that temperature below which CP luminescence is never observed, 18.5 K. Theoretically the triple point is where the excitonic gas, CP, and EHL are in equilibrium, satisfying the Gibbs phase rule.[5] There is no spectroscopic means of determining the density of the gas in equilibrium with the EHL and CP phases. In the next section we estimate the gas phase boundary using thermodynamic arguments.

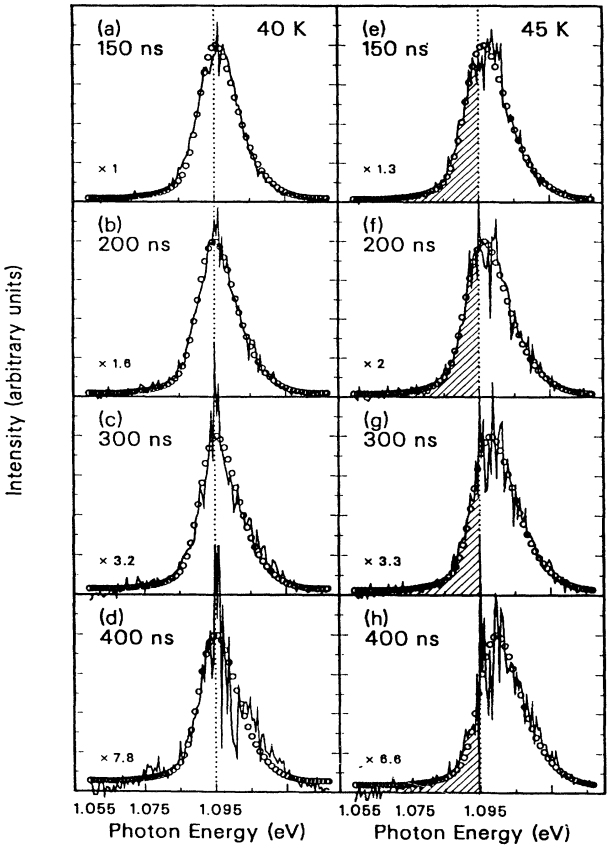

FIG. 14. Comparison of 40 and 45 K time-resolved spectra (with FE and EC components subtracted) obtained at 150, 200, 300, and 400 ns. The dotted line marks the photon energy at 1.095 eV as a guide to the eye. Note the shift to high energies with time for the 45 K spectra.

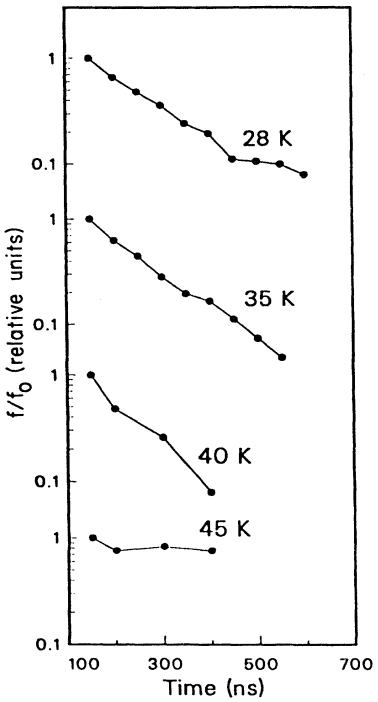

FIG. 15. Relative change of the filling fraction with time at 28, 35, 40, and 45 K. Filling fractions calculated from the least-squares analysis of time-resolved spectra as described in the text. f_0 is the filling fraction at 150 ns.

VI. EXCITONIC PHASE DIAGRAM: EXCITONIC GAS

Thermal equilibrium demands that the chemical potentials of the plasma and all components of the gas phase be equal. The chemical potential of plasmas is determined by the sum of the electron and hole Fermi energies relative to the bottom of the renormalized band. These are easily determined spectroscopically. It is convenient to measure the chemical potential relative to the exciton band edge. Defined in this way, the chemical potential μ is just the negative of the plasma-exciton work function $\mu=-\phi=\Delta_{\rm FE}^0-\Delta E_{BB}+E_F^e+E_F^h$, where $\Delta_{\rm FE}^0$ is the exciton binding energy, ΔE_{BB} is the band renormalization as described in Sec. IV, and E_F^e and E_F^h are the electron and hole Fermi energies. To be more specific, in the calculations that follow, $\mu=-\phi_{\rm EHL}$ for $T<18.5$ K and $\mu=-\phi_{\rm CP}$ for $18.5<T<45$ K, where $\phi_{\rm EHL(CP)}$ is the EHL(CP) exciton work function measured spectroscopically. Having fixed the chemical potential, the total gas density can be written as the sum of exciton, trion, molecule, and free-carrier densities using Richardson-type equations[24,50]

$$
\begin{aligned}
n_{\rm FE}&=g_{\rm FE}N_{\rm FE}e^{\mu/k_BT}\,,\\
n_f&=g_fN_fe^{(\mu+\Delta_f)/2k_BT}\,,\\
n_t&=g_tN_te^{(3\mu-\Delta_{\rm FE}+2\Delta_t)/2k_BT}\,,\\
n_{\rm EM}&=g_{\rm EM}N_{\rm EM}e^{(2\mu+\Delta_{\rm EM})/k_BT}\,,
\end{aligned}
\tag{9}
$$

where $N_i=(m_ik_BT/2\pi\hbar^2)^{3/2}$ is the quantum density, g_i is the degeneracy, and Δ_i is the binding energy of each

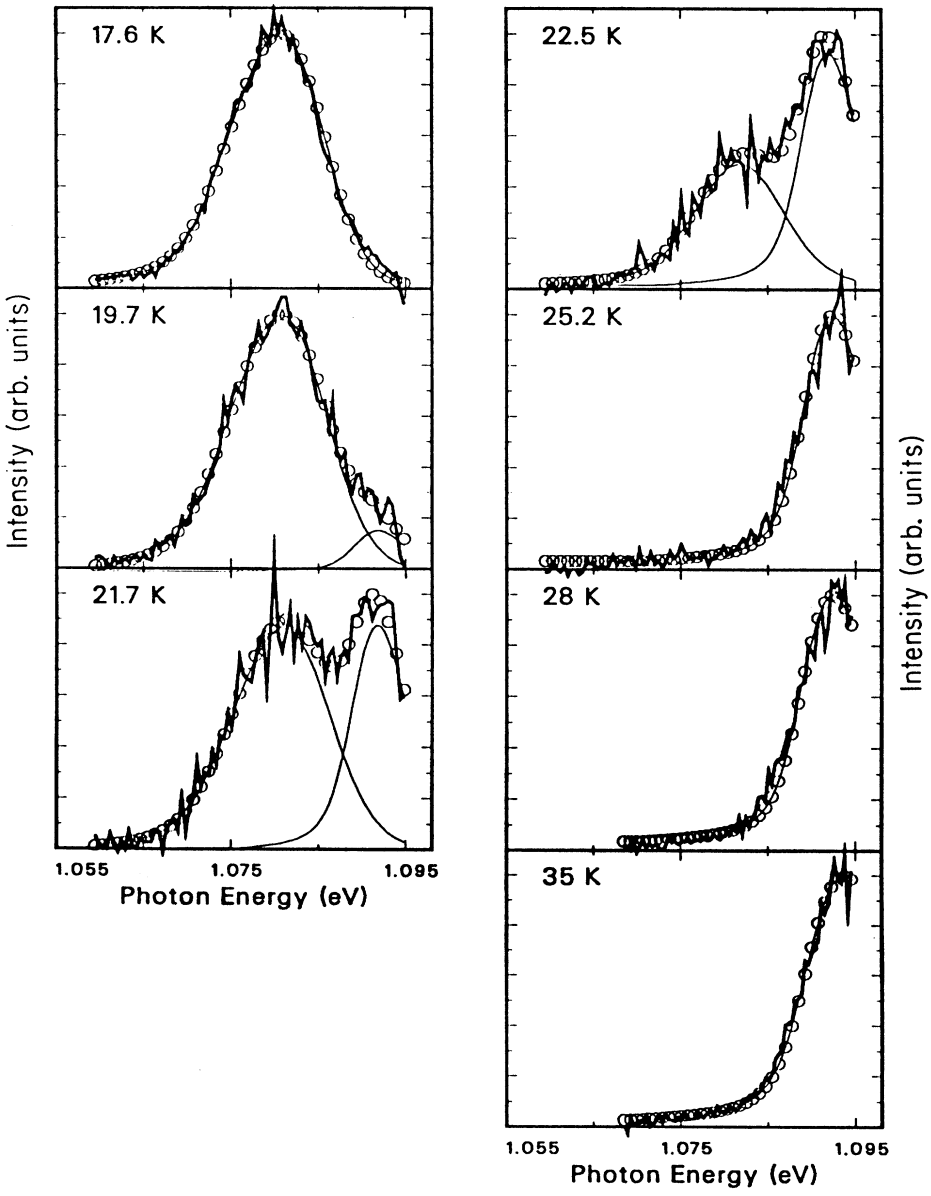

FIG. 16. Temperature dependence of time-resolved luminescence spectra (thick lines) 150 ns after the laser pulse with FE and EC components subtracted as described in the text. Open circles are least-squares fits composed of EHL ($T<24.5$ K) and/or CP ($T>18.5$ K) components. The thin lines are EHL and/or CP line shapes which are summed to produce the spectral fits. The equilibrium parameters of the EHL and CP phases may be found in Fig. 17.

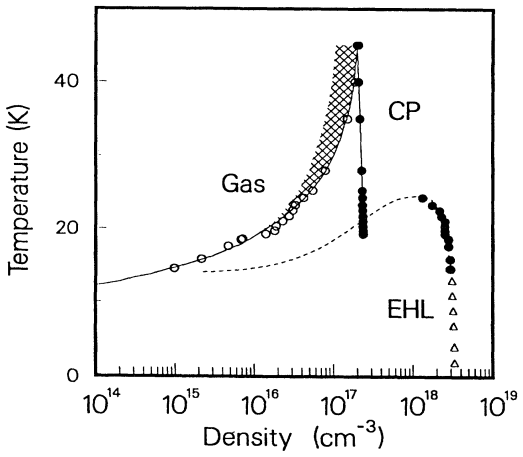

FIG. 17. Proposed phase diagram of excitonic matter in Si. Solid circles are densities of the EHL and the CP determined from the data. The dashed line is a Guggenheim fit to the EHL densities. Open circles and the shaded region are calculated total gas pair densities, as described in the text. Triangles are low-temperature EHL data from Ref. 35.

TABLE I. Mass (m_i), degeneracy (g_i), and binding energy (Δ_i) of free carriers (1), excitons (2), trions (3), and excitonic molecules (4) used in the calculations of Sec. VI.

i	m_i/m_{FE}	g_i	Δ_i (meV)
1	0.49	4.9	$-\Delta_{FE}/2$
2	1	24	0
3	1.50	39.8	1.22
4	2	66	1.22

species (FE denotes free excitons, f denotes free electrons or holes, t denotes positive or negative trions, and EM denotes excitonic molecules). Since the free electrons or holes, and positive or negative trions have different degeneracies and masses, we use the geometric averages $m_f=\sqrt{m_e m_h}$, $g_f=\sqrt{g_e g_h}$, $m_t=\sqrt{m_{t+}m_{t-}}$, and $g_t=\sqrt{q_{t+}g_{t-}}$. The relevant masses and degeneracies used in this calculation are listed in Table I. (Note that the parameters listed in Table I are calculated assuming that only the heavy-hole band is occupied, so that a comparison can be made with the calculations of Refs. 14, 24, and 25.)

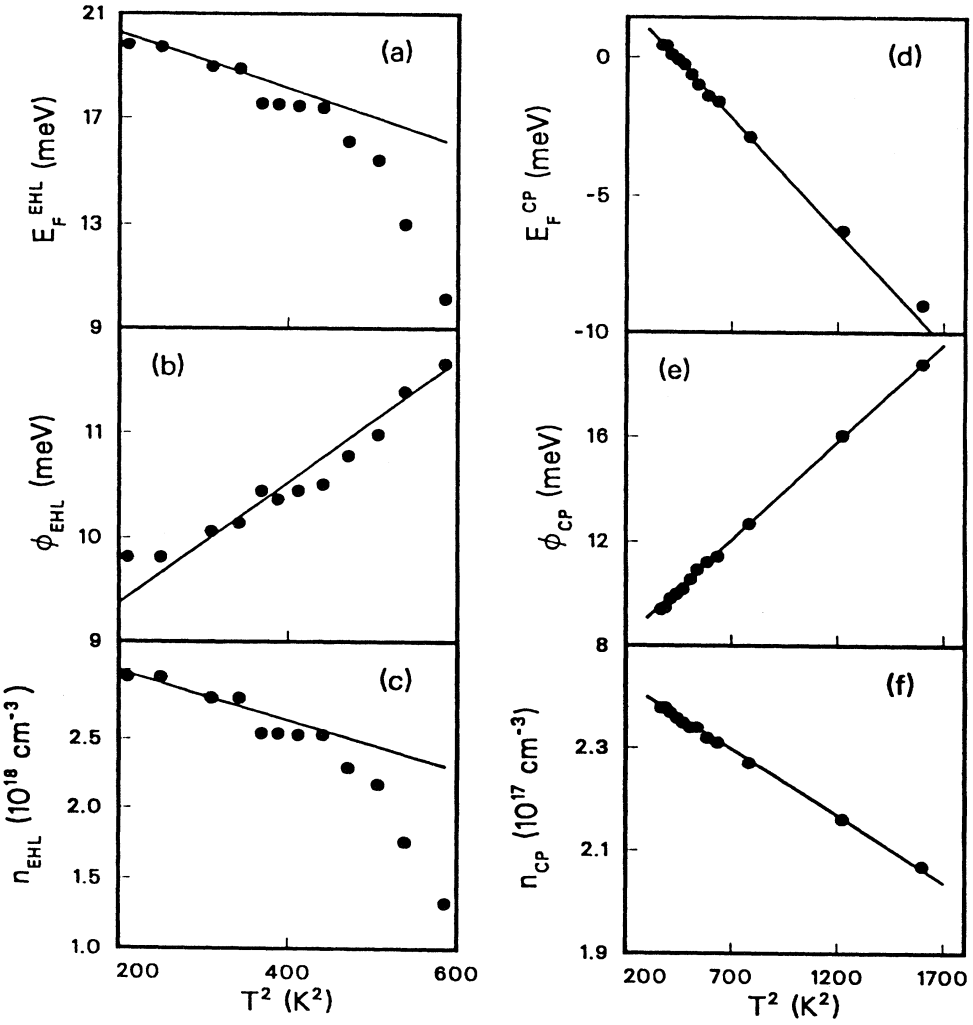

FIG. 18. Equilibrium parameters of EHL and CP phases versus T^2. Straight lines are the best fit to the data as described in the text.

Consider a gas in equilibrium with EHL at $T \ll T_c(\mathrm{LG})$. The gas density is very low (Fig. 17) and the FE is the dominant component of the gas phase. At high temperatures, the gas density rises exponentially with temperature and so the fraction of three- and four-particle complexes relative to the FE becomes much larger. This is because of the exponential dependence expected for the EM and trion density with the FE density: $n_t \propto n_{\mathrm{FE}}^{3/2}$ and $n_{\mathrm{EM}} \propto n_{\mathrm{FE}}^2$. In addition, the expressions for the free-carrier and trion densities in Eq. (9) depend on the free-exciton binding energy. Reduction of the exciton binding energy from screening of the Coulomb potential by charged particles should increase the expected density of these species and so such effects must be considered in the calculation of the gas density.

The effects of screening on the exciton binding energy can be estimated by replacing the potential in the hydrogenic Hamiltonian by the screened (Yukawa) potential

$$\phi(r) \propto \frac{e^2 e^{-q_{\mathrm{DH}} r}}{\kappa r} . \tag{10}$$

Here r is the electron-hole interparticle spacing, κ is the static dielectric constant, e is the unit of electronic charge, and q_{DH} is the Debye-Huckel screening wave vector $[q_{\mathrm{DH}}=(8\pi e^2 n/\kappa k_B T)^{1/2}]$. To first order in perturbation theory the exciton binding energy becomes

$$\Delta_{\mathrm{FE}}(n)=\Delta_{\mathrm{FE}}^0(1-2q_{\mathrm{DH}}a_{\mathrm{FE}}) , \tag{11}$$

where a_{FE} is the excitonic Bohr radius. If one includes a quantum correction originating from the thermal broadening of the electron de Broglie wavelength one obtains

$$\Delta_{\mathrm{FE}}(n)=\Delta_{\mathrm{FE}}^0\left[1-\frac{2q_{\mathrm{DH}}a_{\mathrm{FE}}}{1+C\Lambda q_{\mathrm{DH}}}\right] , \tag{12}$$

where $\Lambda=h/\sqrt{2\pi m k_B T}$ is the de Broglie wavelength of an electron and C is a constant estimated by Kremp and co-workers to be $\approx\frac{1}{8}$.[7-10]

Using Eqs. (9) and (12) we must solve the coupled equations

$$\begin{aligned} n_c(\mu,\Delta_{\mathrm{FE}})&=n_f(\mu,\Delta_{\mathrm{FE}})+n_t(\mu,\Delta_{\mathrm{FE}}) , \\ n_g(\mu,\Delta_{\mathrm{FE}})&=n_f(\mu,\Delta_{\mathrm{FE}})+n_{\mathrm{FE}}(\mu) \\ &\quad +3n_t(\mu,\Delta_{\mathrm{FE}})+2n_{\mathrm{EM}}(\mu) , \end{aligned} \tag{13}$$

where $\Delta_{\mathrm{FE}}=\Delta_{\mathrm{FE}}(n_c)$ is given by Eq. (12) and n_c equals the charge density. These coupled equations can be solved numerically for a given constant chemical potential and temperature. In this calculation the chemical potential is fixed by the plasma and determined through line-shape analysis, while the temperature is measured by the carbon resistor. The only free parameter used to determine the gas density is C. If we demand that $n_g=n_{\mathrm{CP}}$ at the critical temperature $T_c(\mathrm{MI})=45$ K, then $C\approx 0.2$. The phase diagram determined in this way is shown in Fig. 17. The solid circles are the experimentally determined plasma densities and the open circles are the total pair gas densities n_g with $C=0.2$. The shaded region to the left of the open circles shows the effect of increasing C to 0.6. No solution is possible to the coupled equations if $C<0.18$.

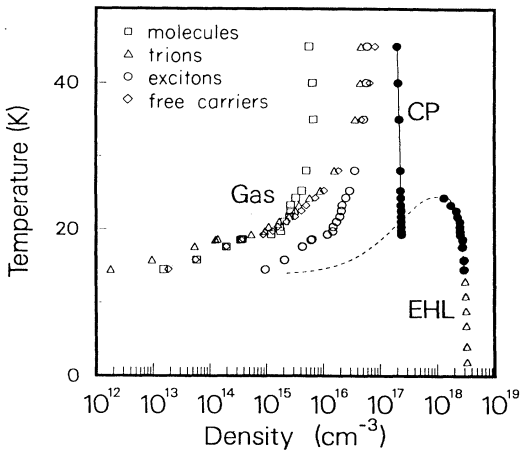

FIG. 19. Phase diagram of Fig. 18 with densities of each component of the gas plotted. Open symbols are the densities of excitonic molecules (open squares), trions (open triangles), free-electron–hole pairs (open diamonds), and free excitons (open circles). Triangles on the high-density section of the phase diagram are low-temperature EHL data from Ref. 35.

The partial pair density of each phase which composes the gas are shown in Fig. 19. Note that near the upper critical temperature $T_c(\mathrm{MI})$ the free-carrier density is as large as the exciton density. Luminescence from these free-electron–hole pairs is extremely weak since the expected luminescence intensity of a plasma at such densities is over an order of magnitude lower than that of the CP.

It is remarkable that over the entire temperature range 0–40 K only four luminescence line shapes—the FE, the EC, the CP, and the EHL—account for all the data. This agreement would seem to be fortuitous since the phase diagram of Figs. 17 and 19 predict that in the temperature range 18.5–24.5 K, EHP's with densities between the CP phase boundary and the EHL saturated gas density should be allowed. One might expect to observe luminescence from plasmas with densities covering this entire range, as pointed out by Hernandez.[30] In the next section we discuss reasons why this intermediate-density EHP luminescence is not observed and study the dynamics of the initial formation of the EHL and CP phases from the hot plasma created during the laser pulse.

VII. DYNAMICS OF FORMATION AND DECAY OF EHL'S AND CP'S

The analysis of spectra at time <50 ns introduces significant complications. Since the particles are nonthermalized, the lattice temperature can no longer be assumed in the fits and, in addition, temperature gradients should rule out the possibility of a single elevated fit temperature to describe all the phases. In the analysis that follows we shall make the following simplifying assumptions.

(i) At times <9 ns the spectra are almost pure EHP

line shapes and the temperature and density can be fit directly. We have determined through line-shape analysis that the temperatures of these early plasmas are ≈ 45 K for lattice temperatures $T_3 < T < T_c$(LG).

(ii) At times >9 ns the temperature of the EHP lines are assumed to decrease exponentially from ≈ 45 K to the lattice temperature with a 6-ns time constant determined previously by Steranka and Wolfe.[38–40] Steranka and Wolfe performed similar luminescence experiments on silicon above the liquid-gas critical temperature, but used higher excitation levels, allowing a more precise determination of the temperature because only small contributions to the luminescence from the excitonic gas were present.

(iii) The EHL condenses from a lower-density hot plasma and so the formation of the EHL is easily determined by the growth of luminescence at low photon energies as described in Sec. III. The density of the EHL at these early times is determined by spectroscopic analysis. From the density of the EHL one can determine the temperature through the temperature-density relation of the phase diagram.

(iv) Remarkably, all the fits to these early time spectra are consistent with exciton and complex line shapes at the lattice temperature. Presumably the excitonic components diffuse out farther into the crystal at early times. Only one parameter, the intensity of the excitonic component, determines both FE and EC line shapes, as we have related their intensities by the scaling relation described in Sec. III.

Of course, an analysis performed on such spectra using the above assumptions can only be a rough guide to the true situation where one would expect continuous temperature and density gradients. Nevertheless, as can be seen in Figs. 20 and 21, the above simplifications work well. For the 21.7 K luminescence in Fig. 20, the spectra for $t \leq 9$ ns can be fit by a combination of a single 45 K plasma line shape with FE and EC line shapes at the lattice temperature. At 12 ns one notices a definite downward shift of the luminescence on the low-energy side, which signals the initial condensation of the EHL. The EHL seems to form initially at a temperature and density

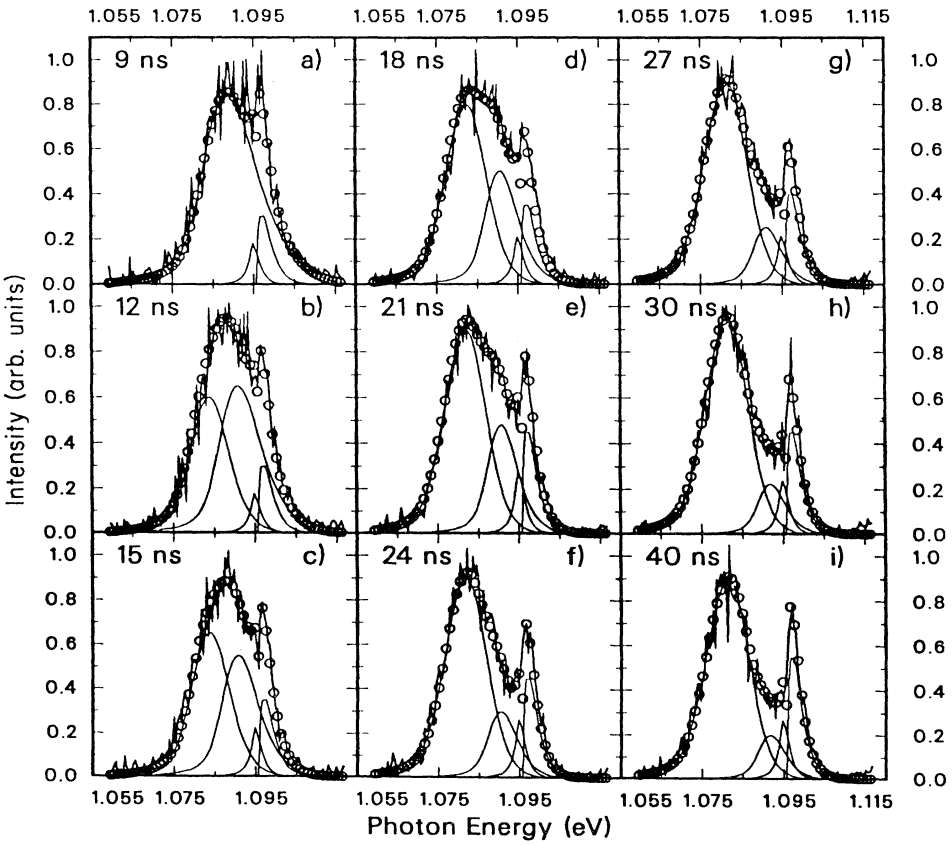

FIG. 20. Time-resolved spectra at 21.7 K. Open circles are fits composed of the EHL, the EHP and/or the CP, the EC and the FE, as described in the text. The parameters are as follows: (a) 9 ns, n_{EHP} (45 K)$=8.2\times10^{17}$ cm^{-3}; (b) 12 ns, n_{EHP} (35.8 K)$=4.2\times10^{17}$ cm^{-3}, n_{EHL} (24.2 K)$=1.3\times10^{18}$ cm^{-3}; (c) 15 ns, n_{EHP} (30.3 K)$=3.8\times10^{17}$ cm^{-3}, n_{EHL} (24.2 K)$=1.3\times10^{18}$ cm^{-3}; (d) 18 ns, n_{CP} (26.9 K) $=3.5\times10^{17}$ cm^{-3}, n_{EHL} (23 K)$=1.8\times10^{18}$ cm^{-3}; (e) 21 ns, n_{CP} (24.8 K)$=3.3\times10^{17}$ cm^{-3}, n_{EHL} (22.5 K)$=2.1\times10^{18}$ cm^{-3}; (f) 24 ns, n_{EHP} (23.6 K)$=3.3\times10^{17}$ cm^{-3}, n_{EHL} (22.5 K) $=2.1\times10^{18}$ cm^{-3}; (g) 27 ns, n_{EHP} (22.9 K)$=2.8\times10^{17}$ cm^{-3}, n_{EHL} (21.7 K)$=2.3\times10^{18}$ cm^{-3}; (h) 30 ns, n_{CP} (22.4 K) $=2.3\times10^{17}$ cm^{-3}, n_{EHL} (21.7 K)$=2.3\times10^{18}$ cm^{-3}; and (i) 40 ns, n_{CP} (22 K) $=2.4\times10^{17}$ cm^{-3}, n_{EHL}(21.7 K)$=2.3\times10^{18}$ cm^{-3}.

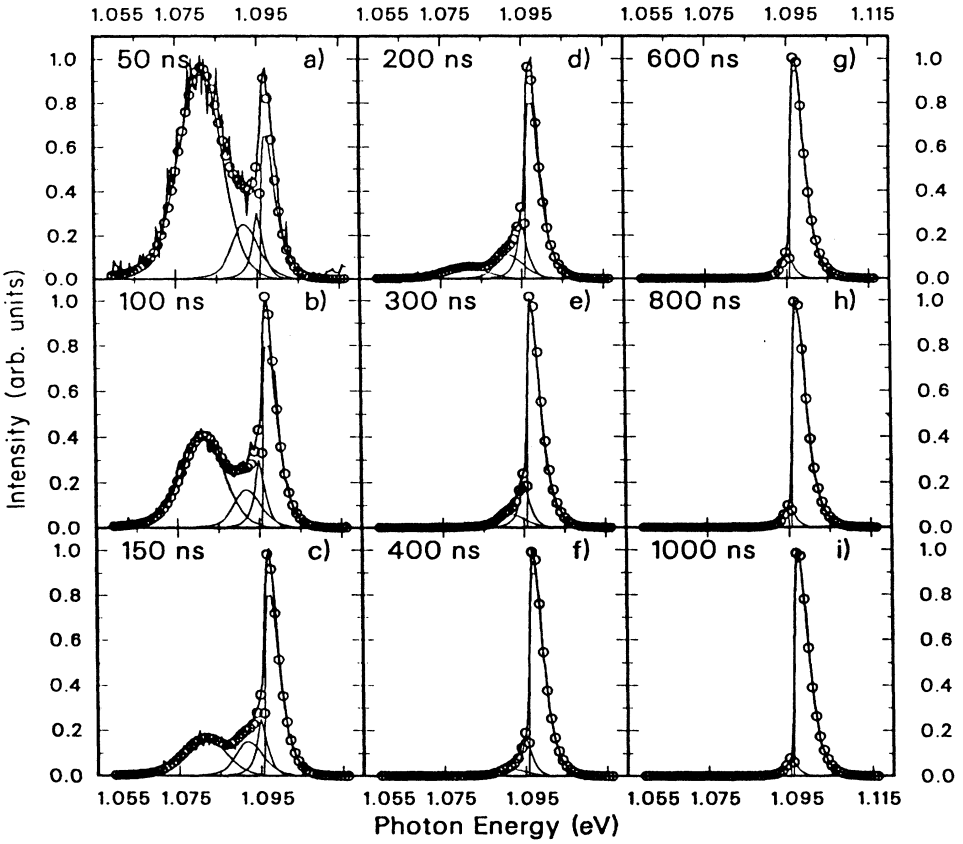

FIG. 21. Time-resolved spectra at 21.7 K. Open circles are fits composed of the EHL, the EHP and/or the CP, the EC, and the FE as described in the text. Equilibrium parameters of the EHL and CP phases may be found in Fig. 17. The other parameters are (a) 50 ns, (b) 100 ns, (c) 150 ns, (d) 200 ns, (e) 300 ns, (f) 400 ns, (g) 600 ns, (h) 800 ns, and (i) 1000 ns.

very near the liquid-gas critical point, as would be expected. The condensation of the liquid consumes a significant fraction of the electron-hole pairs, so the hot plasma is left at a significantly reduced density. The liquid cools rapidly over the next 15 ns to the lattice temperature, thereby increasing its density. Note that for 12 ns $< t < 27$ ns the EHP density is significantly above the equilibrium CP density, but relaxes to the CP density by 27 ns. The temperature of the EHP decreases exponentially with a 6-ns time constant, until it reaches the lattice temperature at 50 ns. For times greater than 50 ns (see Fig. 21), all the species are at the lattice temperature.

The average pair density can be estimated by calculating the total integrated intensity divided by the observed volume the electron-hole pairs occupy in the crystal. The absolute scale of this density is determined by fits to the 9-ns spectrum of Fig. 20(a), where almost all of the luminescence is from the EHP. We make the assumption that the density of the EHP at 9 ns is close to the average electron-hole pair density. In Fig. 22 the average pair density is plotted as a function of time and in the inset the evolution of the total pair density and plasma temperature is plotted as a trajectory on the phase diagram. Even at the earliest times, the average pair density is well below the EHL equilibrium density. By 50 ns, when all the pairs are thermalized, the average density has decreased to the CP density, and over the lifetime of the CP, the average pair density decreases further until the saturated gas density is reached. This implies that the EHL never exists in equilibrium with the surrounding gas, but instead evaporates into a rarefied excitonic gas

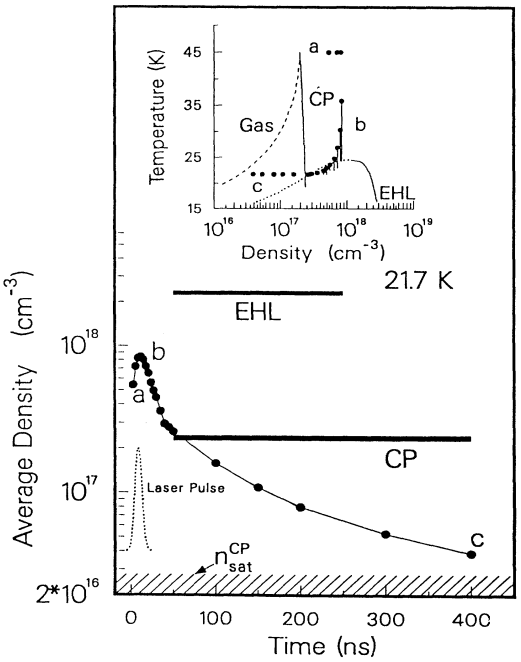

FIG. 22. Average pair density estimated from the spectral intensity and spatial profiles. Two length and the position of bars labeled EHL and CP indicate the lifetime and the density of these components. The shaded region is an estimate of the saturated gas density in equilibrium with the CP. Inset: position of these data points on the new phase diagram. Cooling occurs within $t \leq 50$ ns. A distribution of plasma density and temperature occurs at earlier times.

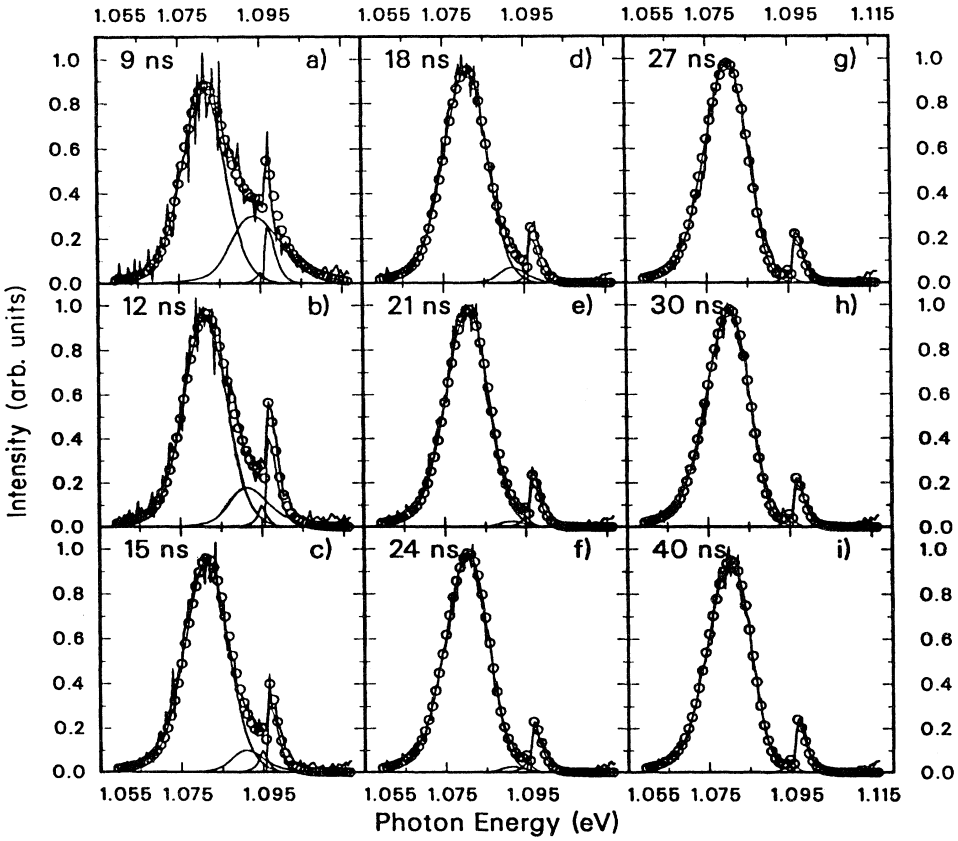

FIG. 23. Time-resolved spectra at 15.8 K. Open circles are fits composed of the EHL, the EHP, and/or the CP, the EC, and the FE as described in the text. The parameters are as follows: (a) 9 ns, n_{EHP} (45 K)$=3.4\times10^{17}$ cm^{-3}, n_{EHL} (2.17 K)$=2.3\times10^{18}$ cm^{-3}; (b) 12 ns, n_{EHP} (33.5 K)$=3.7\times10^{17}$ cm^{-3}, n_{EHL} (21.7 K)$=2.3\times10^{18}$ cm^{-3}; (c) 15 ns, n_{EHP} (26.5 K)$=3.2\times10^{17}$ cm^{-3}, n_{EHL} (21.7 K)$=2.3\times10^{18}$ cm^{-3}; (d) 18 ns, n_{CP} (22.3 K)$=2.3\times10^{17}$ cm^{-3}, n_{EHL}(19.7 K)$=2.5\times10^{18}$ cm^{-3}; (e) 21 ns, n_{CP} (19.75 K)$=2.4\times10^{17}$ cm^{-3}, n_{EHL} (19.7 K)$=2.5\times10^{18}$ cm^{-3}; (f) 24 ns, n_{CP} (18.5 K)$=2.4\times10^{17}$ cm^{-3}, n_{EHL} (17.6 K)$=2.8\times10^{18}$ cm^{-3}; (g) 27 ns, n_{EHL} (15.8 K)$=2.9\times10^{18}$ cm^{-3}; (h) 30 ns, n_{EHL} (15.8 K)$=2.9\times10^{18}$ cm^{-3}; and (i) 40 ns, n_{EHL} (15.8 K)$=2.9\times10^{18}$ cm^{-3}.

whose density is virtually an order of magnitude less than the expected EHL equilibrium saturated gas. This nearly explains the absence of any EHL luminescence with density greater than the CP equilibrium density. On the other hand, the CP does seem to evaporate into an excitonic gas whose density is comparable to the CP saturated gas. In addition, the CP phase appears to exist only as long as the average pair density is greater than the CP saturated gas density, which is consistent with the phase diagram.

In contrast, note that in the 15.8 K spectra of Fig. 23, the liquid is present at even the earliest times, but nonetheless forms from a hot, lower-density 45 K plasma. The EHL temperature is still well above the lattice temperature, but after the laser turns off, the liquid quickly thermalizes and increases its density. As the temperature of the hot plasma decreases, the density of the EHP also decreases until it reaches the CP phase boundary, after which time the CP quickly thermalizes and disappears after cooling below the triple point. In all cases which we have analyzed in this way, no plasmas are observed with density lower than the CP phase boundary and no low-density plasmas are observed at temperatures below the triple point. Thus, even during the brief time during thermalization of the electron-hole pairs to the lattice temperature, the plasma densities are constrained by the phase diagram.

VIII. SUMMARY

We have presented an extensive study of the dynamics of EHL and EHP formation and decay in the transcritical temperature region for excitons in Si. Photoluminescence from a condensed phase of EHP with density one-tenth that of the EHL is observed at temperatures between 18.5 and 45 K. This condensed plasma decays with time while maintaining a constant density. The filling fraction of the CP is seen to decrease by an order of magnitude during its lifetime, indicating the formation of droplets. Above 45 K the EHP decays homogeneously to lower density with time, while the filling fraction remains constant, confirming the absence of the CP.

A two-critical-point phase diagram for excitons in Si is presented that is consistent with the observations described above. The CP is postulated to be a thermo-

dynamically stable phase which coexists with the excitonic gas. The critical point for formation of the CP is 45±5 K, while that for the formation of the EHL is 24.5±0.5 K. The only temperature where the EHL, the CP, and the excitonic gas are in equilibrium is the triple point at 18.5±0.5 K. Our observations at all temperatures and electron-hole pair densities are consistent with such a phase diagram and all the luminescence can be described assuming the existence of three equilibrium excitonic phases: the EHL, the CP, and the excitonic gas.

ACKNOWLEDGMENTS

We acknowledge useful discussions with A. Simon and with S. Kirch, whose thesis work on Ge precipitated the present study. We thank J. P. Hernandez for fruitful discussions and criticisms, which stimulated our interest in the large-excitonic-complex problem, and M. L. W. Thewalt for communicating his group's results to us in advance of publication. We thank W. Keller of Siemens Ag for the Si crystal. This work was supported in part by the National Science Foundation under Contract No. NSF DMR 85-21444 with facilities supported by the National Science Foundation Materials Research Laboratory Program Grant No. NSF DMR 85-16981. One of us (L.M.S.) acknowledges financial support from the National Science Foundation and the Shell Companies Foundation.

APPENDIX A: EHP LINE SHAPE ANALYSIS

All photoexcited electron-hole plasmas observed in Si display a low-energy tail which is not described by the simple convolution of the electron and hole density of states. Landsberg observed that the void left in the Fermi distribution after an electron and a hole recombine should be quickly filled through particle-particle scattering. This will cause a finite width in the energy of the final state in the recombination process through the Heisenberg uncertainty relation and effectively broaden the resulting luminescence line shape. Landsberg[41] proposed the following expression to calculate the broadened density of states:

$$\rho_{e(h)}(\varepsilon)=\int_0^\infty \frac{\Gamma_{e(h)}(\varepsilon')/2\pi}{(\varepsilon-\varepsilon')^2+[\Gamma_{e(h)}(\varepsilon')/2]^2} \times \mathcal{D}_{e(h)}(\varepsilon')f_{e(h)}(\varepsilon')d\varepsilon' , \quad \text{(A1)}$$

where $\mathcal{D}_{e(h)}(\varepsilon)\propto\sqrt{\varepsilon}$ and $f_{e(h)}(\varepsilon)=[e^{(\varepsilon-E_F^{e(h)})/k_BT}+1]^{-1}$ with $E_F^{e(h)}$ the electron (hole) Fermi energy. The energy-dependent Lorentzian broadening is greatest at the bottom of the electron or hole band and decreases monotonically to zero at the Fermi surface. The simplest form for this energy-dependent broadening is[43]

$$\Gamma_{e(h)}(\varepsilon)=\Gamma^0_{e(h)}(1-\varepsilon/E_F^{e(h)}) . \quad \text{(A2)}$$

The broadening parameter $\Gamma^0_{e(h)}$ for a degenerate plasma at $T=0$ K has been calculated by Landsberg to be

$$\Gamma^0_{e(h)}=\frac{8860m}{\kappa^2}\left[\ln(1+x)-\frac{x}{1+x}\right] \text{ meV} , \quad \text{(A3)}$$

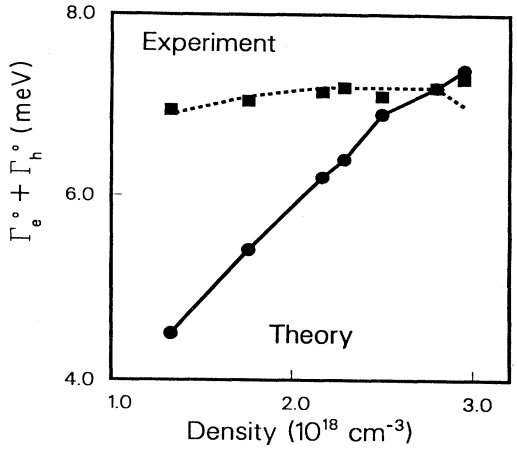

FIG. 24. Sum of the electron and hole broadening parameters ($\Gamma_e^0+\Gamma_h^0$) for Landsberg broadened EHL line shapes as a function of density. Circles are the values obtained through best fits of EHL luminescence for temperatures between 14.5 and 24.5 K. Squares are the theoretically determined values obtained using Eq. (A3).

where $x=(\kappa/2)\sqrt{E_F\pi/4330m}$ with E_F measured in meV.

These expressions adequately describe the broadened EHL line shapes found at low temperatures, but are deficient at higher temperatures. At temperatures greater than 60% of the liquid-gas critical temperature, the EHL density decreases rapidly from 3.0 to 1.0×10^{18} cm^{-3}. The Landsberg theory seriously underestimates the magnitude of the broadening for these lower-density plasmas. In Fig. 24 the sum of the electron and hole broadening parameters ($\Gamma_e^0+\Gamma_h^0$) determined as best fits to the EHL photoluminescence (squares) are compared with the values obtained from Eq. (A3) (circles) over this density-temperature regime. Note that Landsberg's expression [Eq. (A3)] underestimates, by nearly one-half, the broadened line shape for the EHL of density 1.3×10^{18} cm^{-3}. In addition, the Landsberg theory requires that at constant pair density, the broadening of the EHP line shape should decrease rapidly with temperature as the plasma becomes less degenerate. However, this feature of the theory is not supported by experiment. We have found experimentally that the broadening required to describe a 28 K EHP with a density of 5.5×10^{17} cm^{-3} (25-ns spectrum of Fig. 12) is comparable to that observed for the EHL at 14.5 K of density 2.8×10^{18} cm^{-3} [Fig. 7(a)], where the plasma is much more degenerate. Similar behavior can be seen in the spectra of high-temperature plasmas of Refs. 38–40 (cf. Fig. 8 of Ref. 39). These results clearly cannot be accommodated within the Landsberg framework.

In view of the insensitivity of the low-energy tail of the electron-hole plasma over a broad range of densities and temperatures, we are forced to reject the Landsberg interpretation of this ubiquitous broadening in Si. Therefore, in light of the results shown in Fig. 24, we simply fix the value of $\Gamma_e^0+\Gamma_h^0$ to 7 meV, independent of temperature and density. The precise origin of this broadening

remains an open question. Nevertheless, the functional form of the Landsberg broadening formula provides a good (phenomenological) fit to the low-energy tail at all temperatures. In addition, the Landsberg function with temperature-independent broadening appears to fit the other plasmas in the system: the CP phase and its higher-density precursors at early times (see Fig. 12). The densities extracted from the fits to the EHP and the CP are quite insensitive to the specific low-energy broadening chosen. The density is determined almost solely by the position of the line.

To include the possibility of nondegenerate plasmas, we define a pseudo-Fermi energy $E_F^{e(h)*}$ as the energy at which the Fermi distribution is 1% of its value at the bottom of the band:

$$f_{e(h)}(E_F^{e(h)*})/f_{e(h)}(0)=\tfrac{1}{100} \ . \tag{A4}$$

Note that at zero temperature $E_F^{e(h)*}=E_F^{e(h)}$. In addition, Eqs. (A2) and (A3) are modified to[43]

$$\Gamma_{e(h)}(\varepsilon)=\Gamma^0_{e(h)}[1-\gamma_{e(h)}(\varepsilon)] \ , \tag{A5}$$

where

$$\gamma_{e(h)}(\varepsilon)=\frac{\int_0^{\varepsilon} f_{e(h)}(\varepsilon')d\varepsilon'}{\int_0^{\infty} f_{e(h)}(\varepsilon')d\varepsilon'} \tag{A6}$$

and

$$\Gamma^0_e/\Gamma^0_h=E_F^{e*}/E_F^{h*} \ . \tag{A7}$$

At low temperatures, Eqs. (A5) and (A6) closely approximate the form of Eq. (A2). In this way, the broadened density of states $\rho_{e(h)}(\varepsilon)$ may be calculated using Eqs. (A1) and (A5)–(A7) and the theoretical EHP line shape written

$$I(h\nu)=I_0\int \rho_e(\varepsilon_e)\rho_h(\varepsilon_h)\delta[h\nu-(E_g-\Delta_{BB}-\hbar\omega_{\mathrm{LO/TO}}+\varepsilon_e+\varepsilon_h)]d\varepsilon_e d\varepsilon_h \ . \tag{A8}$$

The theoretical EHP luminescence line shape depends on three parameters: density, temperature, and $\Gamma^0_e+\Gamma^0_h$. By holding the latter fixed at $\Gamma^0_e+\Gamma^0_h=7$ meV we are able to completely determine the EHP luminescence line shape with the fewest number of parameters, namely, the temperature and density.

APPENDIX B: THEORETICAL ESTIMATES OF THE RENORMALIZED GAP AT NONZERO TEMPERATURES

Previous pulsed-laser experiments on Si (Ref. 15) and Ge (Refs. 36 and 51) have shown that the spectral position of the exciton luminescence line shape is quite independent of density. Since the exciton binding energy decreases with increasing charge density from screening effects, there must be a compensating shift in the continuum band edge. From the density-dependent exciton binding energy derived in Eq. (11) we obtain the following expression for the band-gap renormalization in the dilute density limit using Debye-Huckel screening:

$$\Delta E_{BB}(n)=2q_{\mathrm{DH}}a_{\mathrm{FE}}\Delta^0_{\mathrm{FE}} \ . \tag{B1}$$

Therefore, the band-gap renormalization increases exponentially (with half power) as the square root of the charge density. The validity of this expression may be extended to high densities by including a quantum correction from thermal broadening of the electronic wave function [see Eq. (12)]:

$$\Delta E_{BB}(n)=\frac{2q_{\mathrm{DH}}a_{\mathrm{FE}}\Delta^0_{\mathrm{FE}}}{1+C\Lambda q_{\mathrm{DH}}} \ . \tag{B2}$$

Note that the Debye-Huckel form [Eq. (B1)] is regained in the low-density limit. We have now determined the band renormalization energy in both the low- (Debye-Huckel) and high- (Vashishta-Kalia) density limits. Unfortunately, the CP density occurs in exactly the intermediate-density regime where neither form is strictly expected to be applicable, yet we use the VK expression [Eqs. (2) and (3), and solid line of Fig. 25] to analyze the CP luminescence line shape. How accurate are the results of Vashishta and Kalia in this low-density region?

Rosler, Zimmermann, and Richert[52] and Kraeft *et al.*[53] have attempted to calculate from first principles the exchange and correlation energy for non-zero temperature carrier distributions in semiconductors for all densities. Rosler, Zimmermann, and Richert[52] and Kraeft *et al.*[53] use a Padé approximation to obtain an analytical expression that reconstructs their numerical results, but depends only on knowing the exchange-correlation ener-

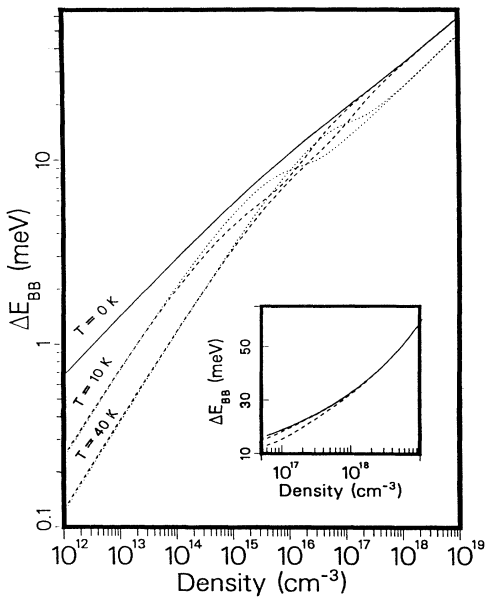

FIG. 25. Theoretical calculations of the band-gap renormalization as a function of electron-hole pair density. The solid line is the $T=0$ K calculation of Vashishta and Kalia (Ref. 26), Eqs. (2) and (3) in the text. Dotted lines are the nonzero temperature calculations of Rosler, Zimmermann, and Richert[52] and Kraeft *et al.*[53] at 10 and 40 K. Dashed lines are a phenomenological approximation combining limiting forms of Refs. 25, 52, and 53, given by Eqs. (6) and (7) in the text. Inset: blowup of the region of interest for all electron-hole plasmas considered in this discussion. Solid and dashed lines are the same as before.

gy in the limiting cases of complete nondegeneracy (Debye-Huckel) and strong degeneracy (VK-like expression). Unfortunately, as can be seen from the dotted lines in Fig. 25, the calculation of Rosler, Zimmermann, and Richert[52] severely underestimates the band-gap renormalization for degenerate plasmas and so their expression is not compatible with the observed EHL luminescence.

To estimate the accuracy of the Vashishta-Kalia expression, we use the Padé approximation of Rosler, Zimmermann, and Richert[52] but replace their limiting degenerate exchange-correlation function by the experimentally verified expression of Vashishta and Kalia [Eq. (3)]. To be more specific, we use the function

$$\Delta E_{BB}=\frac{8\bar{n}^2\dfrac{\partial(nF_{\rm xc})}{\partial n}-2q_{\rm DH}a_x}{8\bar{n}^2+1+C\Lambda q_{\rm DH}}\ , \tag{B3}$$

where

$$\bar{n}=\frac{3\sqrt{\pi}}{\mathcal{T}^{3/2}r_s^3}\frac{g_e^{-1}+\gamma^{3/2}g_h^{-1}}{(1+\gamma)^{3/2}} \tag{B4}$$

is a measure of the degeneracy, $F_{\rm xc}$ is given by Eq. (3), and $\mathcal{T}=k_BT/\Delta_{\rm FE}^0$ is the temperature in units of excitonic Rydbergs. The electron and hole degeneracies are $g_e=6$ and $g_h=2$, while $\gamma=m_e/m_h=1.47$. The dashed lines of Fig. 25 show that this expression at 10 and 40 K coincides with the Vashishta-Kalia result [Eqs. (2) and (3), and solid line of Fig. 25] at high densities and the Debye-Huckel result [Eq. (B1)] at low densities. The inset of Fig. 25 shows the same result on an expanded linear scale, but without the results of Rosler, Zimmermann, and Richert. For the observed CP band-gap renormalization, the Padé approximation [Eqs. (B3) and (B4)] at 40 K yields a density of 3×10^{17} compared with 2×10^{17} cm^{-3} for the $T=0$ Vashishta-Kalia result. (Note that at lower temperatures this difference is smaller.) This indicates the possible systematic errors in determining the CP density.

APPENDIX C: THEORETICAL ESTIMATE OF THE DENSITY OF LARGE COMPLEXES

It has been suggested[30,33] that the origin of the CP luminescence is in fact from the decay of "large" excitonic complexes (LC's) composed of more than two pairs. Though it is quite possible that such complexes do contribute to the luminescence, we believe such contributions to be much smaller than the low-density plasma luminescence. The problem of predicting the relative density of large complexes is quite difficult. Though Wang and Kittel[54] have predicted that large complexes in multivalley semiconductors are bound when the holes are very massive, no such predictions are available when the electron and hole masses are compatible. Since the valence band if fourfold degenerate, we will assume that only complexes with four or fewer holes are bound. This results from the expense one pays in kinetic energy to add the fifth hole due to the Pauli exclusion principle. Following the procedure followed in Sec. VI, we can immediately write down the following Richardson-type equations[24,50] for all the complexes with fewer than five holes:

TABLE II. Mass (m_i), degeneracy (g_i), and binding energy (Δ_i) of free carriers (1), excitons (2), and small (3 and 4) and large (5–8) complexes used in the calculations of Appendix C.

i	$m_i/m_{\rm FE}$	g_i	Δ_i (meV)
1	$\frac{1}{2}$	6.9	$-\Delta_{\rm FE}/2$
2	1	48	0
3	$\frac{3}{2}$	137.9	1.36
4	2	396	1.36
5	$\frac{5}{2}$	590.3	5.19
6	3	880	5.19
7	$\frac{7}{2}$	660	11.53
8	4	495	11.53

$$\begin{aligned}
n_5&=g_5N_5e^{(5\mu/2-\Delta_{\rm FE}/2+\Delta_5)/k_BT}\ ,\\
n_6&=g_6N_6e^{(3\mu+\Delta_6)/k_BT}\ ,\\
n_7&=g_7N_7e^{(7\mu/2-\Delta_{\rm FE}/2+\Delta_7)/k_BT}\ ,\\
n_8&=g_8N_8e^{(4\mu+\Delta_8)/k_BT}\ ,
\end{aligned} \tag{C1}$$

where μ is the chemical potential measured relative to the exciton band edge, $N_i=(m_ik_BT/2\pi\hbar^2)^{3/2}$ is the quantum density, g_i is the degeneracy, Δ_i is the binding energy of each species, and i denotes the number of particles in the complex. For simplicity we include only singly charged ions (e.g., $i=5$ is combination of three electrons and two holes and vice versa).

We would like to compare these theoretical results with what is observed in the photoluminescence experiments described above. Since the effective volumes of EC and CP luminescence are approximately the same, the ratio of the CP and EC luminescence intensities is equivalent to the ratio of LC and EC densities if one assumes all the luminescence we previously attributed to CP is from large complexes. To calculate the density ratio theoretically, it is necessary to know the chemical potential for each spectrum considered since the CP line

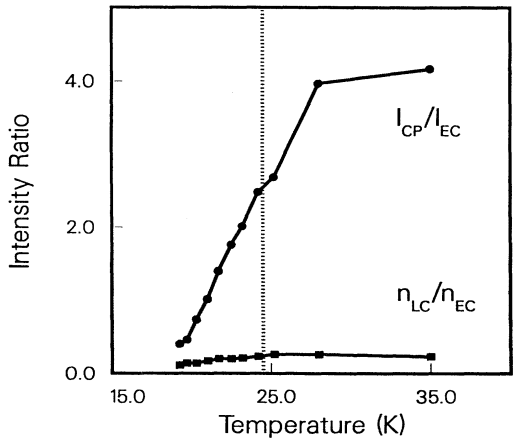

FIG. 26. Comparison of the theoretically determined ratio of large to small complexes ($n_{\rm LC}/n_{\rm EC}$) to the experimental ratio of CP to EC luminescence intensity ($I_{\rm CP}/I_{\rm EC}$).

shape can no longer be assumed to fix the chemical potential. For simplicity, we will assume that below T_c(LG) the chemical potential is fixed by the EHL ($\mu = -\phi_{\rm EHL}$ for $T < 24.5$ K). To determine the chemical potential in the absence of the EHL it is convenient to compare the free-exciton intensity $I_{\rm FE}$ and effective volume $V_{\rm FE}$ at temperatures above and below T_c(LG). The density of excitons is determined by computing $I_{\rm FE}/V_{\rm FE}$ and comparing with the value obtained 150 ns after the laser pulse at 21.7 K. The absolute calibration of the exciton density is obtained by assuming that the excitonic chemical potential, and hence the density, is fixed by the liquid at 21.7 K. Interestingly, the chemical potentials obtained in this fashion for spectra observed at temperatures above the EHL critical point correspond closely to the values obtained spectroscopically from the CP luminescence spectrum (this fact actually supports the CP interpretation).

Recently, direct evidence of the existence of large complexes has been observed by Steele, McMullan, and Thewalt[33] using the Green luminescence produced by direct four-particle recombination of the photoexcited carriers. Values for the binding energies (relative to separated excitons) of large complexes obtained from such experiments are used in the present calculation (see Table II). [Note that the EM binding energy used in this calculation (1.36 meV) is different from that used in Sec. VI (1.22 meV), which was determined from ir spectra. A discussion of this small discrepancy may be found in Ref. 55. For consistency, in this calculation all binding energies are determined from the Green photoluminescence.] For simplicity we use the binding energy of the three- and four-exciton complexes to describe those of the five- and seven-particle ionic species. Since the large complexes are composed of both light and heavy holes, for consistency we compute the degeneracies of all species ($i = 1-8$) assuming that both hole bands are occupied. The masses of each species are assumed to be simple multiples of the excitonic mass: $m_i = (i/2)m_{\rm FE}$. Since the five- and seven-particle complexes include both positive and negative ions, the degeneracies of these particles are calculated as the geometric average. The relevant parameters of each species are listed in Table II.

We compute the density of LC self-consistently as in Sec. VI. The total pair density of large (LC) and small (EC) complexes is given by

$$n_{\rm LC} = 5n_5 + 3n_6 + 7n_7 + 4n_8 \ , \tag{C2}$$

$$n_{\rm EC} = 3n_t + 2n_{\rm EM} \ , \tag{C3}$$

with $\Delta_{\rm FE}(n_c)$ given by Eq. (12) and

$$n_c = n_f + n_t + n_5 + n_7 \ . \tag{C4}$$

The results of this calculation of $n_{\rm LC}/n_{\rm EC}$ are shown in Fig. 26 as squares. For comparison the intensity ratio of CP to EC luminescence is also shown as circles. Note that near the triple point (18.5 K) the expected luminescence intensity of the LC is comparable to the actual CP intensity. However, the intensity of the CP rises sharply above the background luminescence as the temperature increases. By 28 K, the ratio of CP to LC luminescence intensity should be 8 or greater. It is difficult to see how a combination of large complexes, even if the CP luminescence line shape could be adequately explained, could mimic the sharp temperature dependence of the CP relative to the EC above the triple point.

*Present address: Dept. of Physics, University of Cincinnati, Cincinnati, OH 45221-0011.

[1]N. F. Mott, *Metal-Insulator Transitions* (Taylor & Francis, London, 1974).
[2]F. J. Rodgers, H. C. Graboske, Jr., and D. J. Harwood, Phys. Rev. A **1**, 1577 (1970).
[3]E. A. Guggenheim, J. Phys. Chem. **13**, 253 (1945); *Thermodynamics* (Wiley, New York, 1967).
[4]T. M. Rice, in *Proceedings of the Twelfth International Conference on the Physics of Semiconductors, Stuttgart, 1974,* edited by M. H. Pilkuhn (Teubner, Stuttgart, 1974), p. 23.
[5]H. B. Callen, *Thermodynamics* (Wiley, New York, 1960), p. 163.
[6]L. D. Landau and G. Zeldovich, Acta Phys. Chim. URSS **18**, 194 (1943).
[7]W. D. Kraeft, K. Kilimann, and D. Kremp, Phys. Status Solidi B **72**, 461 (1975).
[8]W. Ebeling, W. Kraeft, and D. Kremp, in *Ergebnisse der Plasmaphysik und der Gaselektronik,* edited by R. Kompe and M. Steenback (Academie-Verlag, Berlin, 1976), Vol. 5.
[9]W. Ebeling, W. D. Kraeft, D. Kremp, and K. Kilimann, Phys. Status Solidi B **78**, 241 (1976).
[10]R. Zimmermann, K. Kilimann, W. D. Kraeft, D. Kremp, and G. Ropke, Phys. Status Solidi B **90**, 175 (1978).
[11]I. Balslev, Phys. Status Solidi B **101**, 749 (1980).
[12]J. Shah, M. Combescot, and A. H. Dayem, Phys. Rev. Lett. **38**, 1497 (1977).
[13]A. F. Dite, V. D. Kulakovskiĭ, and V. B. Timofeev, Zh. Eksp. Teor. Fiz. **72**, 1156 (1977) [Sov. Phys. JETP **45**, 604 (1977)].
[14]A. Forchel, B. Laurich, J. Wagner, W. Schmid, and T. L. Reinecke, Phys. Rev. B **25**, 2730 (1982).
[15]A. Forchel, B. Laurich, G. Moersch, W. Schmid, and T. L. Reinecke, Phys. Rev. Lett. **46**, 678 (1981).
[16]P. L. Gourley and J. P. Wolfe, Phys. Rev. B **24**, 5970 (1981).
[17]J. C. Hensel, T. G. Phillips, G. A. Thomas, and T. M. Rice, in *Solid State Physics,* edited by H. Ehrenreich, F. Seitz, and D. Turnbull (Academic, New York, 1977), Vol. 32.
[18]K. Cho, Opt. Commun. **8**, 412 (1973).
[19]P. L. Gourley and J. P. Wolfe, Phys. Rev. B **20**, 3319 (1979).
[20]M. L. W. Thewalt and J. A. Rostworowski, Solid State Commun. **25**, 991 (1978).
[21]S. G. Elkomoss and A. S. Amer, Phys. Rev. B **11**, 2925 (1975).
[22]Z. A. Insepov and G. E. Norman, Zh. Eksp. Teor. Fiz. **69**, 1321 (1975) [Sov. Phys. JETP **42**, 674 (1975)].
[23]B. Stebe and G. Munschy, Solid State Commun. **17**, 1051 (1975).
[24]G. A. Thomas, J. B. Mock, and M. Capizzi, Phys. Rev. B **18**, 4250 (1978).

[25]G. A. Thomas and T. M. Rice, Solid State Commun. **23**, 359 (1977).
[26]P. Vashishta and R. K. Kalia, Phys. Rev. B **25**, 6942 (1982).
[27]L. M. Smith and J. P. Wolfe, Phys. Rev. Lett. **57**, 2314 (1986).
[28]L. M. Smith and J. P. Wolfe, *Proceedings of the Eighteenth International Conference on the Physics of Semiconductors, Stockholm, 1986* (World Scientific, Singapore, 1987), p. 1409.
[29]L. M. Smith and J. P. Wolfe, Phys. Rev. Lett. **58**, 2823 (1987).
[30]J. P. Hernandez, Phys. Rev. Lett. **58**, 2822 (1987).
[31]L. J. Schowalter, F. M. Steranka, M. B. Salamon, and J. P. Wolfe, Phys. Rev. B **29**, 2970 (1984).
[32]S. H. Simon, S. J. Kirche, and J. P. Wolfe, Phys. Rev. B **46**, 10 098 (1992).
[33]A. G. Steele, W. G. McMullan, and M. L. W. Thewalt, Phys. Rev. Lett. **59**, 2899 (1987).
[34]R. J. Elliot, Phys. Rev. **108**, 1384 (1957).
[35]R. B. Hammond, D. L. Smith, and T. C. McGill, Phys. Rev. Lett. **35**, 1535 (1975).
[36]G. A. Thomas, A. Frova, J. C. Hensel, R. E. Miller, and P. A. Lee, Phys. Rev. B **13**, 1692 (1976).
[37]M. A. Tamor and J. P. Wolfe, Phys. Rev. Lett. **44**, 1703 (1980).
[38]F. M. Steranka and J. P. Wolfe, Phys. Rev. Lett. **53**, 2181 (1984).
[39]F. M. Steranka and J. P. Wolfe, Phys. Rev. B **34**, 1014 (1986).
[40]J. P. Wolfe, J. Lumin. **30**, 82 (1985).
[41]P. T. Landsberg, Phys. Status Solidi **15**, 623 (1966); Proc. Phys. Soc. London Sect. A **62**, 806 (1949).
[42]R. W. Martin and H. L. Störmer, Solid State Commun. **22**, 523 (1977).
[43]V. D. Kulakovskiĭ, V. B. Timofeev, and V. M. Èdel'shteĭn, Zh. Eksp. Teor. Fiz. **74**, 372 (1978) [Sov. Phys. JETP **47**, 193 (1978)].
[44]W. Schmid, Phys. Status Solidi B **94**, 413 (1979).
[45]Jagdeep Shah and A. H. Dayem, Phys. Rev. Lett. **37**, 861 (1976).
[46]M. Combescot, Phys. Rev. Lett. **32**, 15 (1972).
[47]P. Vashishta, S. G. Das, and K. S. Singwi, Phys. Rev. Lett. **33**, 911 (1974).
[48]L. D. Landau and E. M. Lifshitz, *Statistical Physics,* 2nd ed. (Pergamon, London, 1969), p. 154ff.
[49]R. B. Hammond, T. C. McGill, and J. W. Mayer, Phys. Rev. B **13**, 3566 (1976).
[50]M. Combescot, Phys. Status Solidi B **86**, 349 (1978).
[51]I. Balslev and J. Furneux, Solid State Commun. **32**, 609 (1979).
[52]M. Rosler, R. Zimmermann, and W. Richert, Phys. Status Solidi B **121**, 609 (1984).
[53]W. Kraeft, D. Kremp, W. Ebeling, and G. Ropke, *Quantum Statistics of Charged Particle Systems* (Plenum, New York, 1986), p. 193.
[54]J. Shy-Yih Wang and C. Kittel, Phys. Lett. **42A**, 189 (1972).
[55]M. L. W. Thewalt and W. G. McMullan, Phys. Rev. B **30**, 6232 (1984).